Computers and Structures 301 (2024) 107430

Contents lists available at ScienceDirect

Computers and Structures

journal homepage: www.elsevier.com/locate/compstruc

Optimal Uniform Strength Design of Frame and Lattice Structures

Christian Iandiorio [1,*], Daniele Milani [2], Pietro Salvini [3]

Department of Enterprise Engineering, University of Rome "Tor Vergata", Via del Politecnico 1, 00133 Rome, Italy

ARTICLE INFO

Keywords:
Shape Optimization
Uniform-strength
Optimal Design
Frame Structures
Lattice Structures
Structural Optimization

ABSTRACT

This paper provides a procedure to obtain the uniform strength of frame and lattice structures. Uniform strength condition is achieved by performing the shape optimization of all beam elements of the structure. The beam shape which guarantees uniform strength is analytically deduced from the one-dimensional Timoshenko model. The optimization problem presents itself as the search for the zeros of the objective-functions vector, which is a non-linear system of equations representing the kinematic-congruence and forces balance at every node of the structure. The analytical formulation of the optimization problem allows to construct the objective-functions vector without the use of external structural computation, i.e. not recurring to any Finite Element Analysis to accomplish iterations. This latter feature entails a great advantage in terms of computing time required to perform optimization. The proposed analytical formulation allows to directly insert the uniform strength condition into the objective-functions vector, transforming the optimization into an unconstrained problem. Some examples are shown in which the performance of the optimization procedure is discussed in terms of robustness and rate of computational complexity while increasing the degrees of freedom of the structure. The reliability and the quality of the optimization are verified through Finite Element Analysis.

1. Introduction

Structural optimization is engaged in several fields of engineering as mechanical, civil, aerospace, biomedical etc., both for large and small-scale structures [1–3]. In many cases, frame and lattice structures are considered, in which the beams are the main players of the optimization. Some classical examples concern the optimization of bridges, stadium domes, radio towers and bus frames [4–10]. Less classical applications regard the optimization of lattice materials (metamaterials) or space structures [11–16].

The search for an optimum involves the application of advanced mathematical and computational strategies (non-linear programming), which recur to procedures that can be split into two main categories: classic gradient-based methods [17] or heuristic ones [18–20]. Both strategies start with the definition of a representative functional that guides the goodness of the outcomes.

Gradient-based methods attains the optimum according to analytically-based methods, which require computing the derivatives of the objective functions. Some common techniques are: Penalty methods, Sequential Quadratic Programming (SQP), Trust Region, Damped Least-Squares (DLS, also known as Levenberg–Marquardt algorithm), Inscribed Hyperspheres (IHS), and Gradient Projection Method [17,21–23]. All of these suffer the need for an initial guess so that they might reach and stop on an optimum, which could be a local optimum and consequently miss the absolute one.

Heuristic methods follow the idea to set up the optimization process being inspired by observed behaviors in nature. Their main advantage is that they do not require any derivative, which is an expensive operation in terms of computational time. This makes them simple and feasible to use for any optimization problem, non-smooth ones included. Main disadvantages are: the inability to ensure the stationarity of the identified optimal solution and the high number (difficult to foresee) of objective-function calls required to reach an optimum. Among the best-knowns are: Genetic Algorithm (GA), Particle Swarm Optimization (PSO), Ant Colony Optimization (ACO), and Biological Growth Method (BGM) [18,19,24–29].

Previously mentioned optimization techniques are widely used in structural mechanics, which aims to obtain the design of a structure that

* Corresponding author.
E-mail address: christian.iandiorio@uniroma2.it (C. Iandiorio).
[1] ORCID - 0000-0002-0695-4548.
[2] ORCID - 0009-0005-3420-1972.
[3] ORCID - 0000-0002-1852-3737.

https://doi.org/10.1016/j.compstruc.2024.107430
Received 21 December 2023; Accepted 26 May 2024
Available online 1 June 2024

exhibits the best performance in terms of loads, kinematics, mechanical, dimensional, and constraint conditions. The minimization of the weight, dual to best utilization of the material, is the most sought feature in structural optimization; it is usually accompanied by stiffness requirements (i.e. maximum allowed displacements) and stress limitations on some regions of interest. Several scopes may drive the optimal design and can be gathered in the following types: topology, layout, sizing, and shape. First type, the topological, concerns the optimization of the internal arrangement of the structure, generally intended as the optimal number of components (beams for frame structures) keeping unchanged the external kinematic constraints, loads and other design requirements. This is the only optimization procedure, among all above mentioned, that can change the number of components and their connectivity with respect to the baseline, i.e. the structure before optimization [2,7,11,30–40]. In other words, topological optimization achieves the optimum performing a global form-finding.

Layout optimization [7,41–45] is commonly used to minimize stress on frame structures; it operates with a fixed topology (i.e. the same number of components and their connectivity) and modifies the length of the elements and the load application points to get the desired objective.

Sizing optimization typically regards beam/truss structures [7,8,31,36,46–48]; it considers fixed the topology and the length of the components, and acts modifying the size of cross-sections to achieve the best compromise between weight and stiffness.

In some papers, topology and sizing optimization or layout and sizing optimization are performed together or one subsequent the other [7,31,33,36,38,47].

Shape optimization [49–55] is less explored if compared to the previous ones, probably because the geometries resulting at the end of the optimization process are difficult to realize through traditional manufacturing. However, complex and precise geometrical shapes are now easier to produce thanks to the continuous progress in the field of additive manufacturing, not only by polymer but also by metal [56–58], especially with regard to moderate-sized bodies such as machine components. Shape optimization seeks to find the best possible shape for every beam in a structure, that is the scenario investigated in the present paper. From a mathematical point of view, it is much more challenging [59], since the variables that define each attempt may even be continuous functions (dynamic optimization) instead of a table of values (static optimization). Some authors [53–55] address the shape optimization to statically-determinate structures, which results hugely simpler than statically-indeterminate structures.

The aim of the present paper is to encompass shape optimizations on statically-indeterminate frame structures that, to the best knowledge of the authors, have never been investigated in the past. It is interesting to observe that, though beam elements involve a one-dimensional modelling, there are currently no shape optimization procedures that can efficiently work when frames are not statically-determinate, e.g. welded frames.

The procedure here presented allows to obtain the uniform-strength of a planar frame structure performing a (simultaneous) shape optimization of every beam forming the frame to achieve overall uniform strength. Uniform-strength [60–62] is a condition that guarantees a suitable distribution of internal stress, which entails the best use of the material and, therefore, the minimization of the weight.

To reach uniform-strength condition through shape optimization, some numerical procedures [29,63,64] recur to a solid-elements discretization using the Finite Element Method (FEM); obviously, dealing with solid elements implies managing a huge number of degrees of freedom (DOFs) and equations, limiting the number of governing variables driving the optimization. However, a large number of structures can be traced back to frames and thus modelled using beam elements, requiring much fewer DOFs than solid discretization. Using one-dimensional elements, our purpose is to offer an optimization procedure that provides fast results even for large structures, strongly statically-indeterminate.

A recurrent limitation in most structural optimizations, both for gradient-based and heuristic methods, is the need to repeat a Finite Element Analysis (FEA) at each objective function evaluation (Fig. 1a). This continuous call to Finite Element (FE) solvers affects most of the computation time since it requires to suspend the optimization algorithm while waiting for FE results, often provided by external software. To considerably improve speediness, in this paper the search for optimal beam shapes employs an exact analytical deduction based on one-dimensional Timoshenko beam model to perform the tuning of the beam shape along their axes.

The key feature lies in the fact that the optimization problem turns into the search for the zeros of the non-linear system of analytically defined objective functions.This peculiarity allows to update the optimization workspace, which in our procedure includes the structural modelling, non-recurring to any external structural computation (e.g. FEA) at each iteration (Fig. 1). This significantly reduces the required time for the optimization, even for structures formed by a huge number of elements. On the other hand, it is useful to specify that the optimization procedure here outlined primarily focuses on achieving uniform strength. It does not encompass all the technological challenges associated with specific regulations which are postponed to subsequent analyzes after obtaining the optimal design.

It is worth pointing out that the peculiarity of the model is that the resulting shape modulation within each beam is not *a priori* preset, so the complexity of the beam-shape depends on all applied loads (including distributed ones); the uniform-strength is forced as a feature condition on the whole length of every beam.

The approach proposed in this article is particularly well-suited for optimizing machine components, thus within the context of mechanical engineering where optimizing part geometries plays a pivotal role in enhancing lightweight and efficiency.

2. Analytical formulation of the Uniform-Strength beam element

In this section, the governing equations of planar Timoshenko beam are reported for a variable cross-section, symmetrical along one axis (here identified with the y-axis) (Fig. 2). The magnitude of the uniform-strength stress affects the resulting equations, thus presenting the problem in an unusual way. An inverse approach is employed to respect the uniform-strength of whatever load/boundary settings, so that the shape of the beam cross-section is a function of the applied loads. Note that, being the frame structure statically-indeterminate, the element loads are themselves influenced by the geometric shapes of the beams. This relationship yields that this beam model, in terms of force–displacement entanglement, turns highly non-linear.

This paper section aims to develop the formulation of a uniform-strength beam element with two ending nodes; the loads are applied to nodes and/or distributed along the axis. In order to obtain a comprehensible compact formulation, what follows refers to common finite element notations, reference systems and assemblage.

The section is assumed to be non-deformable on its plane [60,65], i.e. without in-plane or out-of-plane warping. The reference system of the element is collinear with the principal axes of inertia and originates at the section centroid of the first node I of the element (Fig. 2).

The 2D displacement field, in the small-displacements regime and Lagrangian description of the motion, is:

$$U(x,y) = u(x) - y\psi(x) \tag{1}$$

$$V(x,y) = v(x) \tag{2}$$

in which U and V are the displacements, along x and y axes, of every point of the beam; u,v and ψ are the cross-section translations (along x and y) and rotation, respectively.

Assuming small strains, the components of the linearized Green

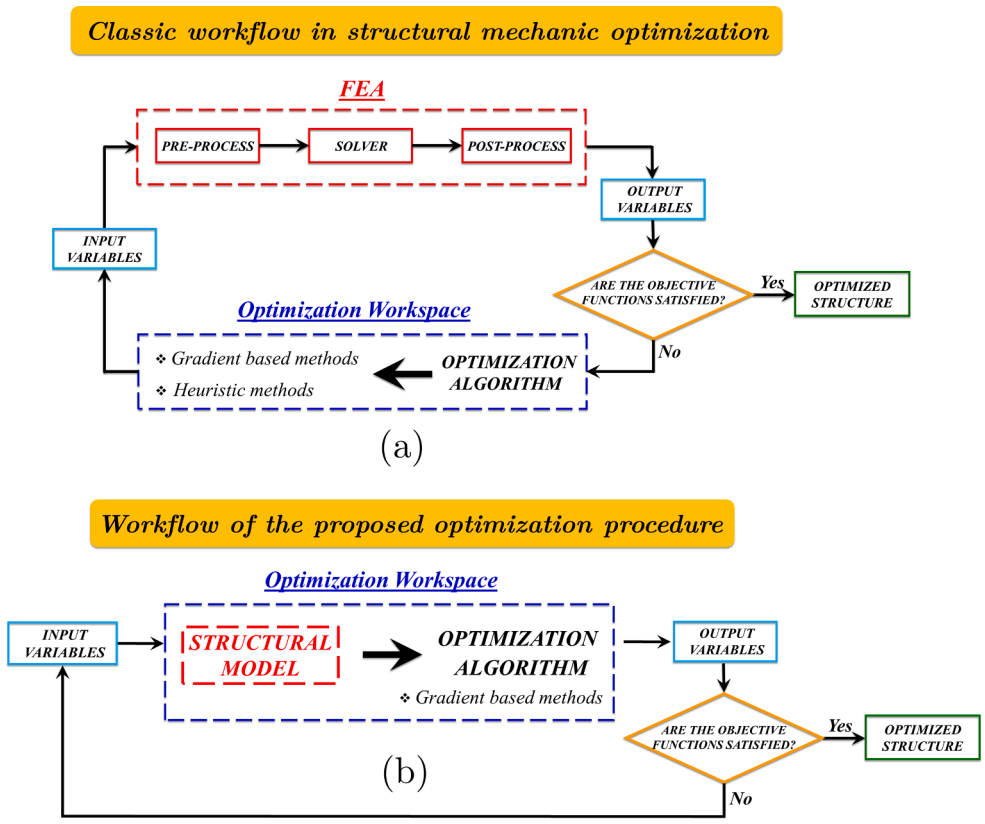

Fig. 1. Work-scheme comparison between classic optimization and the proposed one: (a) Classic workflow; (b) Proposed workflow.

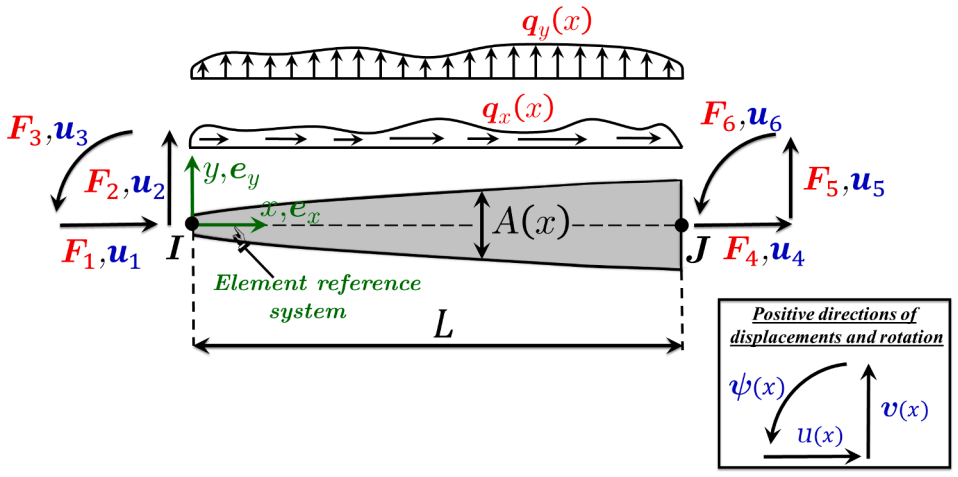

Fig. 2. Notation of forces and displacements of the beam element with a variable shape in its local reference system.

strain tensor are:

$$\varepsilon_x = \frac{\partial U}{\partial x} = u' - y\psi' \tag{3}$$

$$\gamma_{xy} = \frac{\partial U}{\partial y} + \frac{\partial V}{\partial x} = v' - \psi \tag{4}$$

in which compact notation $(\bullet)' = d(\bullet)/dx$ is used.

The material is assumed homogeneous, linear elastic and isotropic, then the axial and shear stresses, using Eqs. (3,4) result as:

$$\sigma_x = E\varepsilon_x = E(u' - y\psi') \tag{5}$$

$$\tau_{xy} = \frac{E}{2(1+\nu)}\gamma_{xy} = G(v' - \psi) \tag{6}$$

where E is the Young's modulus and ν the Poisson's coefficient.

The constant shear strain in Eq. (4) and the shear stresses in Eq. (6) are approximated, due to the missing shear-warping effect of the section. To correct this, on average, a simple way is to impose that the strain energy computed with constant shear stress is equal to the one computed considering the shear stress distribution from the 3D continuum model [66] or with the approximated Jourawsky's approach [60,65]. A shear strain correction factor κ outcomes comparing the two shear stress deductions [60,67], depending on the section's form. This correction factor is used in the Timoshenko beam model to obtain effective shear area

$A_s = A/\kappa$ and effective shear strain $\gamma_{xy}^{eff} = \kappa\gamma_{xy}$.

Resulting internal loads at the section level, namely the normal and shear forces and bending moment, are associated with the previous stresses by:

$$N(x) = \int_{A(x)} \sigma_x dA = EA(x)\ u' \tag{7}$$

$$T(x) = \int_{A_s(x)} \tau_{xy} dA = \frac{GA(x)}{\kappa}\cdot(v' - \psi) \tag{8}$$

$$M(x) = -\int_{A(x)} y\cdot\sigma_x dA = EI(x)\ \psi' \tag{9}$$

where A and I are the (variable with x) area and moment of inertia of the cross-section.

From eq.s (5–9) and the given latter correction, the governing equations of kinematics and stresses are:

$$\begin{cases} u'(x) = \dfrac{N(x)}{EA(x)} \\ \cdot \\ \psi'(x) = \dfrac{M(x)}{EI(x)} \\ \cdot \\ v'(x) = \psi(x) + \dfrac{\kappa\, T(x)}{GA(x)} \end{cases} \tag{10}$$

$$\sigma_x(x,y) = \frac{N(x)}{A(x)} - \frac{M(x)}{I(x)}y \tag{11}$$

The shear stresses are not specified since they have no influence on what follows.

To integrate Eqs. (10), two additional information are required: the relationships with the section forces/moment in eq. (7–9) and the nodal/distributed loads, and the shape of the beam cross-section that guarantees uniform-strength.

The straight beam of length L (Fig. 2) is loaded along its axis with the (variable) distributed loads $q_x(x), q_y(x)$ and at its ends (nodes) by concentrated forces and moments. For the sake of clarity, the same notation used for finite elements is adopted, i.e. the nodal forces, moments, translations and rotations are referenced by numerical subscripts.

Applying a virtual cut on the beam (Fig. 3), orthogonal to the beam axis, the relationships between section forces/moment and the applied loads $F_1, \ldots, F_6$ turn out [67,68]:

$$\begin{cases} N(x) = -F_1 - \displaystyle\int_0^x q_x(\tilde{x})d\tilde{x} \\ T(x) = -F_2 - \displaystyle\int_0^x q_y(\tilde{x})d\tilde{x} \\ M(x) = F_2 x - F_3 - \displaystyle\int_0^x (\tilde{x} - x) q_y(\tilde{x})d\tilde{x} \end{cases} \tag{12}$$

in which $\tilde{x}$ is a dummy variable for integration.

Eqs. (12) are obtained by applying equilibrium with respect to the node I, but the same can be easily obtained referring to the forces on the J node using the balance equations between the nodal forces (explicitly reported hereinafter since we refer to both in §4):

$$\begin{cases} F_1 = -F_4 - \displaystyle\int_0^L q_x(x)dx \\ F_2 = -F_5 - \displaystyle\int_0^L q_y(x)dx \\ F_3 = -LF_5 - F_6 - \displaystyle\int_0^L x q_y(x)dx \end{cases} \tag{13}$$

To obtain the shape of the beam the idea is to impose the uniform-strength for the entire beam length. Uniform-strength is an ideal condition aiming to achieve the same maximum stress on all points of a structure. Clearly, this can almost never be exactly achieved except in elementary cases such as truss structure. For general frame structures, stresses caused by bending are dominant; they generate a linear trend of the stress on the section. Therefore, the uniform-strength condition is intended as uniformity of the axial stresses at top or bottom sides, depending on the presence of additional axial loads.

According to the continuum model or Jourawsky's approximation, shear stress vanishes at top and bottom of a beam cross-section (where the magnitude of axial stress is maximum). Therefore, it is reasonable to assume that the presence of shear stress does not affect the shapes of the beam that derive from the condition of uniform-strength.

An inverse approach is carried out to obtain the shape that ensures uniform-strength, imposing the same maximal magnitude of the stress σ_{max} at the top or bottom sides $y = \pm h(x)/2$ along the beam [69]:

$$\sigma_{max} = \frac{|N(x)|}{A(x)} + \frac{|M(x)|}{I(x)}\frac{h(x)}{2} \tag{14}$$

The axial force N and bending moment M of the section are given by Eq. (12), while the *iso*-stress σ_{max} is given as a fixed value throughout the optimization.

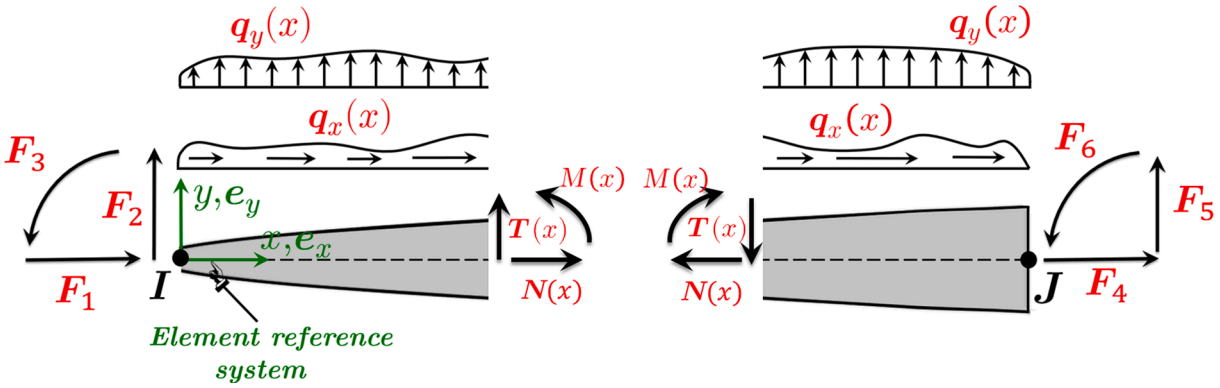

Fig. 3. Equilibrium between nodal forces/moment and internal ones.

Till now, the only limitation regards the one-axis symmetry of the cross section. To go further, it is necessary to specify the type/form of section to deal with. The exact analytical beam shape for some sections of engineering interest is deduced in what follows.

At first, the analysis addresses to the analytical shape of rectangular section beams. The rectangular section in Fig. 4 is assumed to have a known constant width b and an unknown variable height $h(x)$. Substituting into the Eq. (14) the area $A(x) = b\ h(x)$ and the moment of inertia $I(x) = b\ h^3(x)/12$ of this section one obtains:

$$b\sigma_{max}h^2(x) - |N(x)\,|h(x) - 6|M(x)\,| = 0 \tag{15}$$

Solving Eq. (15) with respect to the variable $h(x)$, choosing the positive solution (the only physically acceptable), the section shape (along the x-axis) of the uniform-strength beam with rectangular cross-section (Fig. 4) turns out:

$$h(x) = \frac{|N(x)\,|}{2b\sigma_{max}} + \sqrt{\left(\frac{N(x)}{2b\sigma_{max}}\right)^2 + \frac{6|M(x)\,|}{b\sigma_{max}}} \tag{16}$$

Clearly, many other types of optimized uniform-strength shapes could be found by establishing a law of $b(x)$ variation as a function of the height $h(x)$ variation. The other classical dual way is to keep fixed the height h and vary the width $b(x)$, commonly used in the design of leaf springs.

Another interesting class of solutions concerns the sections that varies homothetically along the beam axis, i.e. sections that can be geometrically scaled using a single variable, further on called h. The area and the moment of inertia of these homothetic sections can be expressed as follow:

$$\begin{cases} A(x) = c_A h^2(x) \\ I(x) = c_I h^4(x) \end{cases} \tag{17}$$

in which c_A and c_I are geometric coefficients depending on the form of the section.

Typical homothetic sections used in frame structures are square (Fig. 5a) and circular (Fig. 5b) ones, both solid or hollow. A void ratio α is introduced to identify them, equal to the ratio between the internal height and the external one ($\alpha = h_i/h_e$) for square sections (Fig. 5a) and the ratio between the internal and external diameter for circular sections (Fig. 5b). The geometric coefficients for the sections in Fig. 5 are:

$$c_A = \begin{cases} (1-\alpha^2) \text{square cross-section (Fig.5a)} \\ \dfrac{\pi(1-\alpha^2)}{4} \text{circular cross-section (Fig.5b)} \end{cases} \tag{18}$$

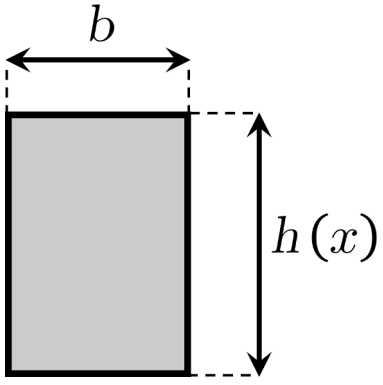

Fig. 4. Rectangular cross-section beam with variable height $h(x)$ and constant width..b

$$c_I = \begin{cases} \dfrac{(1-\alpha^4)}{12} \text{square cross-section (Fig.5a)} \\ \dfrac{\pi(1-\alpha^4)}{64} \text{circular cross-section (Fig.5b)} \end{cases} \tag{19}$$

It is worth to pointing out that for the hollow sections in Fig. 5 with fixed ratio α, the thickness of the section, equal to $(h_e(x) - h_i(x))/2$, varies along the x-axis.

It is necessary to consider the thickness as variable whatever is the section shape. In fact, considering the thickness as fixed, it could be impossible to achieve uniform-strength when the loads reduce significantly, e.g. the case of a beam in which the bending moment $M(x)$ is null at some axis points. At those locations, the section height cannot be reduced more than twice the thickness and consequently the resulting stress drops violating the uniform-strength requirement.

Even more complex sections can be made homothetic, function of a single variable. To make this clearer, consider as example the I-section (IPE) in (Fig. 6) in which the variable that tunes the homothetic section is the height $h(x)$ and all other geometrical information are related to it by scalar quantities $(\alpha_1, \alpha_2, \alpha_3)$. In this case, the two geometric coefficients of the section are:

$$\begin{cases} c_A = 2\alpha_1\alpha_2 + \alpha_3(1-2\alpha_1) \\ c_I = \dfrac{1}{2}\left[\dfrac{{\alpha_1}^3\alpha_2}{3} + \alpha_1\alpha_2(1-\alpha_1)^2 + \dfrac{\alpha_3(1-2\alpha_1)^2}{6}\right] \end{cases} \tag{20}$$

Therefore, it only remains to get the uniform-strength shape formula valid for all homothetic sections; by substituting Eqs. (17) into the Eq. (14), a cubic equation turns out:

$$h^3(x) - \frac{|N(x)\,|}{c_A\sigma_{max}}h(x) - \frac{|M(x)\,|}{2c_I\sigma_{max}} = 0 \tag{21}$$

The discriminant of the cubic eq. (21) is [70]:

$$\Delta(x) = 1 - \frac{16{c_I}^2}{27{c_A}^3\sigma_{max}}\frac{|N(x)\,|^3}{M^2(x)} \tag{22}$$

The solution of a cubic equation depends on the sign of this discriminant, which is an x function; at every sign switch along the axis, the way to achieve the solution changes. However, an important specification holds. Considering the typical values in structural components, the second term at the r.h.s. of Eq. (22) is typically well lower than one. The discriminant in eq. (22) could turn negative or equal to zero only if the bending moment M is several orders of magnitude smaller than the normal stress N. Howe

ver, this implies that the element behaves like a truss. The extremal case of null bending can be kept away since Eq. (21) turns out as a quadratic equation. Given the previous considerations, the discriminant is assumed always positive, avoiding possible switches in the solution.

With a discriminant positive or equal to zero, the unique real solution of the cubic Eq. (21) is:

$$h(x) = \sqrt[3]{-\frac{|M(x)\,|}{4c_I\sigma_{max}}}\left[\sqrt[3]{-1+\sqrt{\Delta(x)}} + \sqrt[3]{-1-\sqrt{\Delta(x)}}\right] \tag{23}$$

If $N(x)$ is null, the previous equation simplifies into:

$$h(x) = \sqrt[3]{\frac{|M(x)\,|}{2c_I\sigma_{max}}} \tag{24}$$

For completeness, the solution with a negative discriminant is reported in the Appendix A.

Being known the uniform-strength shape defined by the solutions

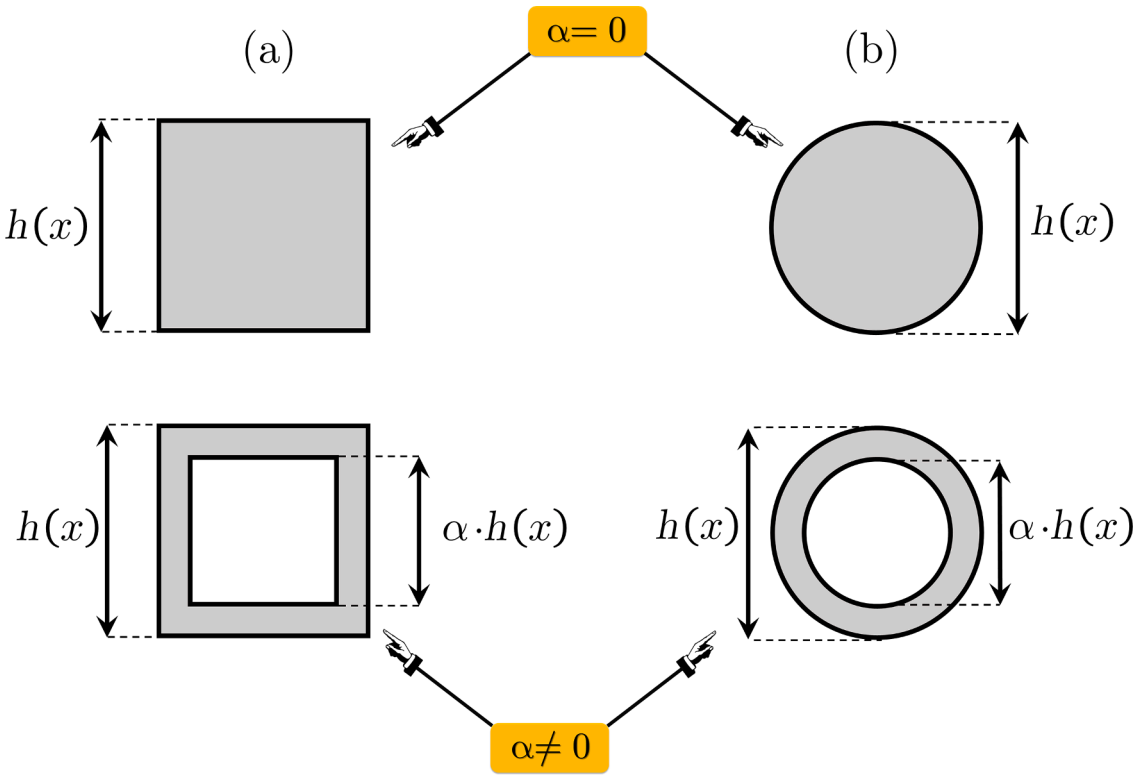

Fig. 5. Solid ($\alpha = 0$) and hollow ($\alpha \neq 0$) cross-sections: (a) square; (b) circular.

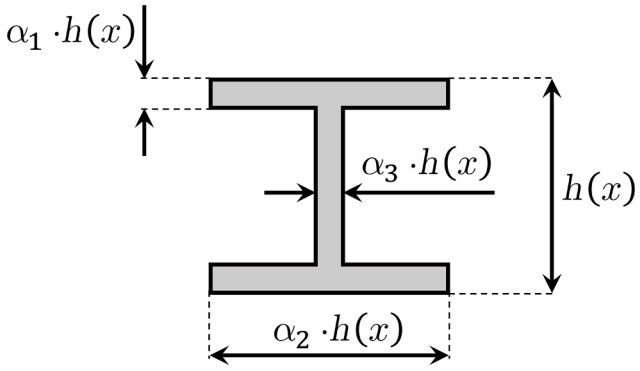

Fig. 6. Homothetic I-section.

$h(x)$ in Eqs. (16 or 23), it is possible to substitute the values of $A(x)$ and $I(x)$ and integrate the kinematic Eqs. (10) to obtain the nodal displacements $(u_1, \cdots, u_6)$ (Fig. 2). The latter are essential to define the objective function of the optimization, hereinafter detailed.

For a statically-indeterminate frame structures, the nodal forces $(F_1, \cdots, F_6)$ that govern the shape of every beam (Eqs. (16,23)) are not known a priori. Therefore, the idea is to solve analytically or numerically the kinematic equations for every beam in its local reference system and, subsequently, to transform them in the global reference system. Referring to the assembled structure, equilibrium conditions and kinematic-congruence require fulfilment at every node. Since the equations, in term of relationships between forces and displacements are non-linear, the satisfaction of the requirements at every node involves an iterative procedure, whose features are explained in details in §4.

The beam shape along its axis (Eqs. (16,23)) may present expressions that are not easy to integrate analytically, especially in the presence of distributed loads. Two analytical solutions, under some assumptions, are investigated in the next section. However, other more complex section forms can always be addressed recurring to numerical integration, as discussed in §3 and shown in §5.

The most important benefit of uniform-strength is that it allows the best use of the material, implying the minimization of the structural weight. To quantify the efficiency achieved, it is possible to introduce the beam efficiency parameter ξ, computed as the ratio between the stored energy and the maximum energy that could (potentially) be accumulated if all material points been subjected to the maximum stress. For beams mainly subjected to bending, unitary efficiency is not reachable, due to the distribution of the stresses, linearly dependent on the distance by respect to neutral axis. If only elastic strain energy associated to bending is taken into account, the efficiency of a beam can be computed as follow:

$$\xi = \frac{1}{\sigma_{max}^2 V(x)} \int_0^L \frac{M^2(x)}{I(x)} dx \tag{25}$$

where $V(x)$ is the beam's volume.

Since the efficiency of the beam cannot reach unity, the measure of efficiency of uniform-strength beams must be compared with that obtained with constant sections. Clearly, the efficiency is function of the loading conditions, and Tab. reports a comparison of the efficiency for a constant and uniform-strength cantilever beam, loaded at the end with a transversal force (i.e. no axial forces $N(x)$ results). The efficiencies in Table 1 are computed analytically through Eq. (25); for uniform-strength beams, the $h(x)$ shape of Eqs. (16,24) are used. Results show that for rectangular and square sections the uniform-strength beams enhance the efficiency for 3 times, considering circular section it assumes the value $3 \bullet \pi^2/4 \approx 7.40$.

3. Displacements' field of the uniform-strength beam element

The aim of this section is to provide the relationship among the nodal forces and displacements of uniform-strength beams. Some analytical and numerical solutions of the beam kinematics, i.e. the integration of

Table 1
Efficiency of constant and uniform-strength cantilever beams loaded at the end with a vertical force.

	Constant rectangular section	*Uniform-strength rectangular section (* Fig. 4*)*	*Constant square (solid or hollow) section (* Fig. 5*a)*	*Uniform-strength (solid or hollow) square section (* Fig. 5*a)*	*Constant circular (solid or hollow) section (*Fig. 5*b)*	*Uniform-strength (solid or hollow) circular section (* Fig. 5*b)*
ξ	$\frac{1}{9}$	$\frac{1}{3}$	$\frac{1}{9}(1+\alpha^2)$	$\frac{1}{3}(1+\alpha^2)$	$\frac{256}{3(32)^2}(1+\alpha^2)$	$\frac{\pi^2 64}{(32)^2}(1+\alpha^2)$

the ODE system of Eqs. (10) considering the uniform-strength shapes derived in §2. The analytical solutions will play a pivotal role in §4, to build up the vector of objective-functions and to carry out the uniform-strength shape optimization of the whole assembled structure.

The analytical integration of the kinematics of the uniform-strength shape is performed, under two restrictive assumptions: the first being the absence of distributed loads $q_x(x), q_y(x)$, and the second is neglecting the influence of the axial forces $N(x)$ on the axial stresses' distribution. In frame structures the stress distribution is bending dominated; as a consequence, the influence of axial forces on stresses is practically negligible. If not, the shape optimization of the beam falls of interest, and the element turns into an almost constant section truss.

If above restrictions cannot be assumed, a numerical integrations of Eqs. (10) is necessary to carry out the optimization process. This approach, fully numerical, is described hereinafter.

The results of analytical and numerical approaches are shown in the examples developed in §5.

3.1. Analytical solution for rectangular sections

Under the absence of distributed loads and neglecting the stresses due to axial forces, the uniform-strength shape of rectangular section with fixed width b (Fig. 4) is obtained applying the third of Eq. (12) into Eq. (16):

$$h(x)=\sqrt{\frac{6|F_2x-F_3|}{b\sigma_{max}}} \tag{26}$$

The equations of the kinematics are:

$$\begin{cases} u'(x)=-\dfrac{F_1}{Eb}\dfrac{1}{h(x)} \\ \psi'(x)=\dfrac{12}{Eb}\dfrac{(F_2x-F_3)}{h^3(x)} \\ v'(x)=\psi(x)-\dfrac{\kappa F_2}{Gb}\dfrac{1}{h(x)} \end{cases} \tag{27}$$

which are obtained using Eqs. (12) into the Eqs. (10) and considering $A(x)=b\,h(x)$ and $I(x)=b\,h^3(x)/12$, where $h(x)$ is made explicit in Eq. (26). For this section, the shear strain correction factor is $\kappa = 6/5$.

The integration of eqs. (27) gives the whole element displacements field:

$$u(x)=c_1-\frac{\sigma_{max}}{3E}\frac{F_1}{|F_2|}h(x) \tag{28}$$

$$\psi(x)=c_2+\frac{4\sigma_{max}}{EF_2}\left|\frac{b\sigma_{max}}{6}h(x)-\frac{F_3}{h(x)}\right|-\frac{4\sigma_{max}}{E}\frac{F_3}{|F_2|}\frac{1}{h(x)} \tag{29}$$

$$v(x)=c_3+c_2x+\frac{4}{3}\frac{b\sigma_{max}{}^2}{EF_2|F_2|}h(x)\left|\frac{b\sigma_{max}}{18}h^2(x)-F_3\right|-\left(\frac{4\sigma_{max}}{E}\frac{F_3}{|F_2|}+\frac{2\kappa F_2}{Gc_N}\right)\frac{b\sigma_{max}}{3|F_2|}h(x) \tag{30}$$

In which the $h(x)$ function, given in Eq. (26), is used in the latter equations to obtain a more compact form. We want to warn up the reader that the integration of the previous equations, even if it may appear simple, actually hides some pitfalls due to the presence of the absolute value appearing in Eq. (26). A useful tip that can be helpful for the reader who wants to deduce the previous solutions is that the signs in Eq. (27) are only due to forces F_1, F_2, F_3, while $h(x)$ is clearly a positive value.

The constants of integration c_1, c_2, c_3 are obtained applying $u(0)=u_1$, $\psi(0)=u_3$, $v(0)=u_2$:

$$c_1=u_1+\frac{\sigma_{max}}{3E}\frac{F_1}{|F_2|}h(0) \tag{31}$$

$$c_2=u_3-\frac{4\sigma_{max}}{EF_2}\left|\frac{b\sigma_{max}}{6}h(0)-\frac{F_3}{h(0)}\right|+\frac{4\sigma_{max}}{E}\frac{F_3}{|F_2|}\frac{1}{h(0)} \tag{32}$$

$$c_3=u_2-\frac{4}{3}\frac{b\sigma_{max}{}^2}{EF_2|F_2|}h(0)\left|\frac{b\sigma_{max}}{18}h^2(0)-F_3\right|+\left(\frac{4\sigma_{max}}{E}\frac{F_3}{|F_2|}+\frac{2\kappa F_2}{Gc_N}\right)\frac{b\sigma_{max}}{3|F_2|}h(0) \tag{33}$$

By computing Eqs. (28–30) at the other end, $x=L$, and using Eqs. (31–33), the relationships between the nodal displacements are revealed:

$$u_4=u_1-\frac{\sigma_{max}}{3E}\frac{F_1}{|F_2|}(h(L)-h(0)) \tag{34}$$

$$\begin{aligned} u_5=u_2+&\left(u_3-\frac{4\sigma_{max}}{EF_2}\left|\frac{b\sigma_{max}}{6}h(0)-\frac{F_3}{h(0)}\right|+\frac{4\sigma_{max}}{E}\frac{F_3}{|F_2|}\frac{1}{h(0)}\right)L+ \\ &+\frac{4}{3}\frac{b\sigma_{max}{}^2}{EF_2|F_2|}\left(h(L)\left|\frac{b\sigma_{max}}{18}h^2(L)-F_3\right|-h(0)\left|\frac{b\sigma_{max}}{18}h^2(0)-F_3\right|\right)+ \\ &-\left(\frac{4\sigma_{max}}{E}\frac{F_3}{|F_2|}+\frac{2\kappa F_2}{Gc_N}\right)\frac{b\sigma_{max}}{3|F_2|}(h(L)-h(0)) \end{aligned} \tag{35}$$

$$\begin{aligned} u_6=u_3+&\frac{4\sigma_{max}}{EF_2}\left(\left|\frac{b\sigma_{max}}{6}h(L)-\frac{F_3}{h(L)}\right|-\left|\frac{b\sigma_{max}}{6}h(0)-\frac{F_3}{h(0)}\right|\right)+ \\ &-\frac{4\sigma_{max}}{E}\frac{F_3}{|F_2|}\left(\frac{1}{h(L)}-\frac{1}{h(0)}\right) \end{aligned} \tag{36}$$

As previously mentioned, the Eqs. (34–36) show a strong non-linear relationship among nodal forces and displacements, considering that the terms F_2 and F_3 appears also in $h(0)$ and $h(L)$. Furthermore, the uniform-strength stress also appears in a non-linear manner, as a consequence, it is not possible to linearly scale the solution with the variation of σ_{max}.

3.2. Analytical solution for homothetic sections

For homothetic sections, keeping the previous mentioned considerations concerning the distributed and axial forces, the uniform-strength shape is:

$$h(x)=\sqrt[3]{\frac{|F_2x-F_3|}{2c_I\sigma_{max}}} \tag{3}$$

obtained applying the third of Eq. (12) into the Eq. (24).

The kinematic equations can be obtained using Eqs. (12) into the Eqs. (10), remembering that.

$A(x)=c_Ah^2(x)$ and $I(x)=c_Ih^4(x)$, where $h(x)$ is given in Eq. (37):

$$\begin{cases} u^{'}(x)=-\dfrac{F_1}{Ec_A}\dfrac{1}{h^2(x)} \\ \psi^{'}(x)=\dfrac{1}{Ec_I}\dfrac{(F_2x-F_3)}{h^4(x)} \\ v^{'}(x)=\psi(x)-\dfrac{\kappa F_2}{Gc_A}\dfrac{1}{h^2(x)} \end{cases} \tag{38}$$

The integration of Eqs. (38) provides:

$$u(x)=c_1-\frac{6c_I\sigma_{max}}{Ec_A}\frac{F_1}{|F_2|}h(x) \tag{39}$$

$$\psi(x)=c_2+\frac{6\sigma_{max}}{EF_2}\left|c_I\sigma_{max}h^2(x)-\frac{F_3}{h(x)}\right|-\frac{6\sigma_{max}}{E}\frac{F_3}{|F_2|}\frac{1}{h(x)} \tag{40}$$

$$v(x)=c_3+c_2x+\frac{18{c_I\sigma_{max}}^2}{EF_2|F_2|}h^2(x)\left|\frac{2}{5}c_I\sigma_{max}h^3(x)-F_3\right|+$$

$$-\frac{18{c_I\sigma_{max}}^2}{E}\frac{F_3}{{F_2}^2}h^2(x)-\frac{6\kappa c_I\sigma_{max}}{Gc_A}\frac{F_2}{|F_2|}h(x) \tag{41}$$

Again, the function $h(x)$ of Eq. (37) is used in these last equations to have more concise formulas.

The constants of integration c_1, c_2, c_3 come out by posing $u(0)=u_1$, $\psi(0)=u_3$, $v(0)=u_2$:

$$c_1=u_1+\frac{6c_I\sigma_{max}}{Ec_A}\frac{F_1}{|F_2|}h(0) \tag{42}$$

$$c_2=u_3-\frac{6\sigma_{max}}{EF_2}\left|c_I\sigma_{max}h^2(0)-\frac{F_3}{h(0)}\right|+\frac{6\sigma_{max}}{E}\frac{F_3}{|F_2|}\frac{1}{h(0)} \tag{43}$$

$$c_3=u_2-\frac{18{c_I\sigma_{max}}^2}{EF_2|F_2|}h^2(0)\left|\frac{2}{5}c_I\sigma_{max}h^3(0)-F_3\right|+\frac{18{c_I\sigma_{max}}^2}{E}\frac{F_3}{{F_2}^2}h^2(0)+$$

$$+\frac{6\kappa c_I\sigma_{max}}{Gc_A}\frac{F_2}{|F_2|}h(0) \tag{44}$$

The nodal displacements relationship are obtained by evaluating Eqs. (39–41) at $x=L$ and using Eqs. (42–44):

$$u_4=u_1-\frac{6c_I\sigma_{max}}{Ec_A}\frac{F_1}{|F_2|}(h(L)-h(0)) \tag{45}$$

$$u_5=u_2+\frac{6\sigma_{max}}{E}\left(\frac{F_3}{|F_2|h(0)}-\left|\frac{c_I\sigma_{max}}{F_2}h^2(0)-\frac{F_3}{F_2h(0)}\right|\right)L+$$

$$+\frac{18{c_I\sigma_{max}}^2}{EF_2|F_2|}\left(h^2(L)\left|\frac{2}{5}c_I\sigma_{max}h^3(L)-F_3\right|-h^2(0)\left|\frac{2}{5}c_I\sigma_{max}h^3(0)-F_3\right|\right)+ \tag{46}$$

$$-\frac{18{c_I\sigma_{max}}^2}{E}\frac{F_3}{{F_2}^2}(h^2(L)-h^2(0))-\frac{6\kappa c_I\sigma_{max}}{Gc_A}\frac{F_2}{|F_2|}(h(L)-h(0))$$

$$u_6=u_3+\frac{6\sigma_{max}}{EF_2}\left(\left|c_I\sigma_{max}h^2(L)-\frac{F_3}{h(L)}\right|-\left|c_I\sigma_{max}h^2(0)-\frac{F_3}{h(0)}\right|\right)+$$

$$-\frac{6\sigma_{max}}{E}\frac{F_3}{|F_2|}\left(\frac{1}{h(L)}-\frac{1}{h(0)}\right) \tag{47}$$

At this point, it is sufficient to know the displacements and forces at node I to obtain the whole internal displacements and forces.

3.3. General numerical solution

The scenario that embraces the presence of distributed loads $q_x(x)$, $q_y(x)$ or the accounting how the stress due to axial load $N(x)$ affects the uniform-strength shape, introduces overwhelming analytical difficulties. Numerical solutions, instead, are always possible, albeit the increase of computational time compared to analytical solutions. The general nodal displacements can be carried out through the numerical integration of Eqs. (10), that using Eqs. (12) appears as:

$$u_4=u_1+\int_0^L\frac{1}{EA(x)}\left[-F_1-\int_0^x q_x(\widetilde{x})d\widetilde{x}\right]dx \tag{48}$$

$$u_5=u_2+\int_0^L\int_0^x\frac{1}{EI(\widetilde{x})}\left[F_2\widetilde{x}-F_3-\int_0^{\tilde{x}}(\widehat{x}-\widetilde{x})q_y(\widehat{x})d\widehat{x}\right]d\widetilde{x}dx+$$

$$+\int_0^L\frac{\kappa}{GA(x)}\left[-F_2-\int_0^x q_y(\widetilde{x})d\widetilde{x}\right]dx \tag{49}$$

$$u_6=u_3+\int_0^L\frac{1}{EI(x)}\left[F_2x-F_3-\int_0^x(\widetilde{x}-x)q_y(\widetilde{x})d\widetilde{x}\right]dx \tag{50}$$

where $\widetilde{x}$ and $\widehat{x}$ are dummy variables. Clearly, $A(x)$ and $I(x)$ are a function of the uniform-strength beam shape $h(x)$ which depends on the form of the beam's cross-section. It is worth to emphasize that Eqs. (48–50) are valid for whatever uniform-strength beam shape which can be obtained as described in §2.

It is straightforward to observe that the use of analytical solutions significantly accelerates the optimization procedure by respect to fully numerical implementations.

4. Optimization procedure

In the previous sections the uniform-strength shape and kinematic equations have been derived. These are functions of the nodal forces F_1, ...,F_6, and the uniform-strength stress σ_{max}.

For a statically-determinate structure the nodal forces do not depend on the shape (i.e. flexibility) of the elements. Therefore, it is easy to obtain the uniform-strength shape of every beam that forms the structure simply applying force balancing. In other words, for statically-determinate structures, the uniform-strength shape is obtained with a one-shot computation (small displacements assumption) and the results are only function of the chosen uniform-strength stress σ_{max}.

For a statically-indeterminate structures, typical in engineering, it is not possible to obtain the nodal forces through simple balancing, inasmuch they depend on the elements' flexibility. Furthermore, in turn, the flexibility of the elements depends on their shapes which are function of the nodal loads. This mutual influence implies to switch to an iterative approach for the finding of uniform-strength shape of every element in the structure. The iterative procedure is stopped when the boundary conditions are satisfied on all beam nodes within a threshold tolerance. These, imposed at every node of the beams, are of kinematic and force type. Clearly, the uniform-strength shapes are affected by the loads and

constraints applied to the entire structure.

For a structure composed of n_{el} elements, a number of $n_{DOFs} = 6 \times n_{el}$ global boundary conditions (equal to the number of degrees of freedom DOFs) are necessary to fix the solution.

The objective is that the structure (already set to be uniform-strength) be kinematically congruent and balanced on all nodes. Therefore, the scalar boundary conditions are stored in the vector of objective-functions $\{\Phi\}$:

$$\{\Phi\} = \begin{Bmatrix} \Phi_1(\{\boldsymbol{F}\},\{\boldsymbol{u}\}) \\ \vdots \\ \Phi_i(\{\boldsymbol{F}\},\{\boldsymbol{u}\}) \\ \vdots \\ \Phi_{n_{DOFs}}(\{\boldsymbol{F}\},\{\boldsymbol{u}\}) \end{Bmatrix}_{n_{DOFs}\times 1} = \begin{Bmatrix} \Phi_1(\{\boldsymbol{F}_I\},\{\boldsymbol{F}_J\},\{\boldsymbol{u}_I\},\{\boldsymbol{u}_J\}) \\ \vdots \\ \Phi_i(\{\boldsymbol{F}_I\},\{\boldsymbol{F}_J\},\{\boldsymbol{u}_I\},\{\boldsymbol{u}_J\}) \\ \vdots \\ \Phi_{n_{DOFs}}(\{\boldsymbol{F}_I\},\{\boldsymbol{F}_J\},\{\boldsymbol{u}_I\},\{\boldsymbol{u}_J\}) \end{Bmatrix}_{n_{DOFs}\times 1} = \begin{Bmatrix} 0 \\ \vdots \\ 0 \\ \vdots \\ 0 \end{Bmatrix} \tag{51}$$

where each row of $\{\Phi\}$, i.e. each condition, is a function of the vectors that collect all nodal forces $\{\boldsymbol{F}\} = \{F_1, F_2 \cdots, F_{n_{DOFs}}\}$ and displacements $\{\boldsymbol{u}\} = \{u_1, u_2 \cdots, u_{n_{DOFs}}\}$.

Note that in the third term of Eq. (51) the forces/displacements associated at the nodes I and J of every beam have been partioned.

For every beam the unknowns are six forces $F_1, \ldots, F_6$ and six displacements $u_1, \ldots, u_6$, but this would imply that the system in Eq. (51) be underdetermined. However, it is fundamental to remember that the forces and displacements at the node J can be deduced from those at node I (Eqs. (13,48–50)).

The forces at the node J are linked to the ones at the node I by the three linear Eqs. (13), i.e. $\{\boldsymbol{F}_J\} = \{\boldsymbol{F}_J(\{\boldsymbol{F}_I\})\}$. The displacements at the node J are non-linear functions of the displacements and forces at the node I, i.e. $\{\boldsymbol{u}_J\} = \{\boldsymbol{u}_J(\{\boldsymbol{u}_I\},\{\boldsymbol{F}_I\})\}$ (one should refers to Eqs. (48–50) if the solution is given numerically or to Eqs. (34–36, 45–47) if it is given analytically). The existence of two relationships between the ending-nodes of every element implies that there are only six unknowns per beam, the three forces F_1, F_2, F_3 and the three u_1, u_2, u_3 at the node I, from which the other forces/displacements at node J derive. Therefore, the system in Eq. (51) results only function of the nodal forces and displacements resulting at the node I, hence it can be reduced as follow:

$$\{\Phi(\{\boldsymbol{F}_I\},\{\boldsymbol{u}_I\})\} = \begin{Bmatrix} \Phi_1(\{\boldsymbol{F}_I\},\{\boldsymbol{u}_I\}) \\ \vdots \\ \Phi_i(\{\boldsymbol{F}_I\},\{\boldsymbol{u}_I\}) \\ \vdots \\ \Phi_{n_{DOFs}}(\{\boldsymbol{F}_I\},\{\boldsymbol{u}_I\}) \end{Bmatrix}_{n_{DOFs}\times 1} = \{0\} \tag{52}$$

which is a (non-linear) system presenting an equal number of unknowns and equations.

To clarify how the objective-functions vector $\{\Phi\}$ is formed, this is fully detailed hereinafter through two examples, which adopt the same well-known numbering of nodes and DOFs usually recurrent on planar frames by finite element codes.

Fig. 7a shows a straight structure, clamped at A, hinged at C and supported at E, with internal rotation release on C. At B and D, where the force F_y and couple M are applied, the adjacent beams are connected each other. Fig. 7b shows the numbering of the nodes, each associated to three DOFs. When two (or more) elements are adjacent as in Fig. 7b, two (or more) elements' nodes geometrically coincides on the structure's nodes; however, since the one of the targets of our objective-functions requires kinematic congruence, it is useful to maintain distinct nodes for distinct elements even if the nodes' location coincide.

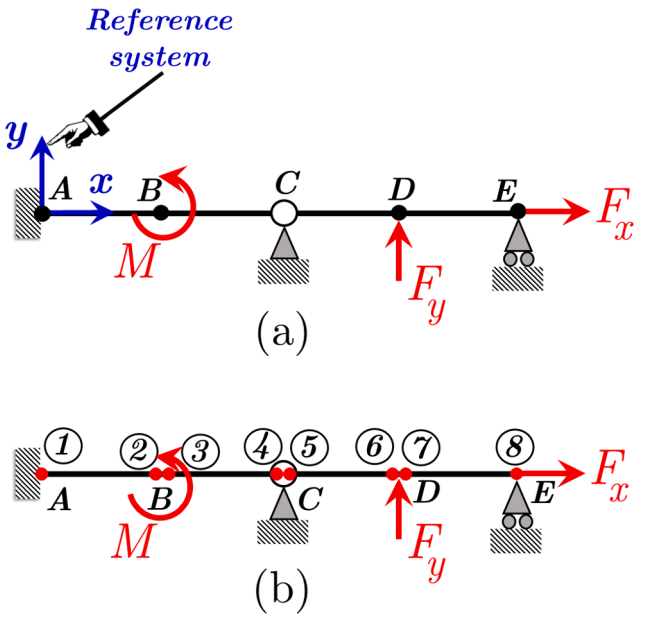

Fig. 7. Supported Structure: (a) Applied forces and kinematic constraints (b) Node numbering.

Table 2
The twenty-four kinematics and forces boundary conditions of the structure in Fig. 7.

Structure's node	*Kinematic B.C.*	*Forces B.C.*
A	$u_1 = 0\ u_2 = 0\ u_3 = 0$	*None*
B	$u_4 - u_7 = 0\ u_5 - u_8 = 0\ u_6 - u_9 = 0$	$F_4 + F_7 = 0\ F_5 + F_8 = 0\ F_6 + F_9 - M = 0$
C	$u_{10} - u_{13} = 0\ u_{10} = 0\ u_{11} - u_{14} = 0\ u_{11} = 0$	$F_{12} = 0\ F_{15} = 0$
D	$u_{16} - u_{19} = 0\ u_{17} - u_{20} = 0\ u_{18} - u_{21} = 0$	$F_{16} + F_{19} = 0\ F_{17} + F_{20} - F_y = 0\ F_{18} + F_{21} = 0$
E	$u_{23} = 0$	$F_{22} - F_x = 0\ F_{24} = 0$

As example, in B, which corresponds to an internal fixed connection, the relative boundary conditions are that the generalized displacements of the two nodes are exactly the same (kinematic congruence). In C, instead, the translational DOFs are the same while the rotational ones are decoupled. Table 2 details all the kinematic and force conditions that form the vector $\{\Phi\}$ for the structure of Fig. 7 which, having four elements, involves twenty-four conditions. As previously discussed, the displacements and forces associated at the "J" nodes 2,4,6,8 (Fig. 7b) are function of the displacements and forces associated at the respective "I" nodes 1,3,5,7, so the vector $\{\Phi\}$ is only function of the DOFs associated at these latter nodes.

In the example of Fig. 7 the global reference system is always collinear with the elements reference systems. For a general frame structure this does not happen; therefore, the displacements and forces require a change of basis to build-up the rows of the vector $\{\Phi\}$ in a unique reference system, the so-called global one. The displacements and forces expressed in the global reference (hereinafter identified by the character "g") can be computed starting from the local one, which starts from the node with the lowest number to the one with the highest number, through the change of basis matrix $[\boldsymbol{R}]$:

$$\begin{Bmatrix} {}^{g}F_1 \\ {}^{g}F_2 \\ {}^{g}F_3 \\ {}^{g}F_4 \\ {}^{g}F_5 \\ {}^{g}F_6 \end{Bmatrix} = \begin{bmatrix} [\boldsymbol{R}]^T & [0] \\ [0] & [\boldsymbol{R}]^T \end{bmatrix} \begin{Bmatrix} F_1 \\ F_2 \\ F_3 \\ F_4 \\ F_5 \\ F_6 \end{Bmatrix} \tag{53}$$

$$\begin{Bmatrix} {}^{g}u_1 \\ {}^{g}u_2 \\ {}^{g}u_3 \\ {}^{g}u_4 \\ {}^{g}u_5 \\ {}^{g}u_6 \end{Bmatrix} = \begin{bmatrix} [\boldsymbol{R}]^T & [0] \\ [0] & [\boldsymbol{R}]^T \end{bmatrix} \begin{Bmatrix} u_1 \\ u_2 \\ u_3 \\ u_4 \\ u_5 \\ u_6 \end{Bmatrix} \tag{54}$$

$$[\boldsymbol{R}] = \frac{1}{L} \begin{bmatrix} {}^{g}x_J - {}^{g}x_I & {}^{g}y_J - {}^{g}y_I & 0 \\ {}^{g}y_I - {}^{g}y_J & {}^{g}x_J - {}^{g}x_I & 0 \\ 0 & 0 & L \end{bmatrix} \tag{55}$$

where ${}^{g}x_I, {}^{g}x_J, {}^{g}y_I, {}^{g}y_J$ are the coordinates of the nodes I and J of the element in the global reference system.

Fig. 8a and Fig. 8b show a frame structure, now developing in a plane, with an assumed node numbering. This structure involves six elements, thus 36 boundary conditions, with multiple connections. Table 3 summarizes all the boundary conditions that form the rows of the vector $\{\Phi\}$, expressed in the global reference system.

In both previous examples, the nodal displacements associated at the second node "J" of every beam is driven by the nodal displacements and forces of the first node "I" applying the analytical or numerical solutions derived in §3.

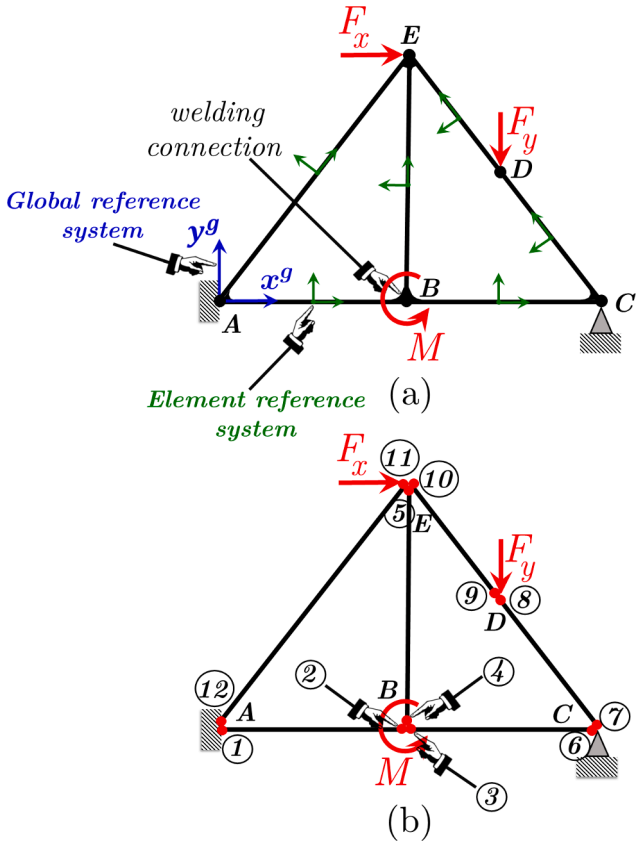

Fig. 8. Frame Structure: (a) Applied forces and kinematic constraints (b) Node numbering.

Table 3
The thirty-six kinematics and forces boundary conditions in the global reference for the structure shown in Fig. 8.

Structure's node	*Kinematic B.C.*	*Forces B.C.*
A	${}^{g}u_1 = 0$ ${}^{g}u_2 = 0$ ${}^{g}u_3 = 0$ ${}^{g}u_{34} = 0$ ${}^{g}u_{35} = 0$ ${}^{g}u_{36} = 0$	*None*
B	${}^{g}u_4 - {}^{g}u_7 = 0$ ${}^{g}u_4 - {}^{g}u_{10} =$ 0 ${}^{g}u_5 - {}^{g}u_8 = 0$ ${}^{g}u_5 - {}^{g}u_{11} =$ 0 ${}^{g}u_6 - {}^{g}u_9 = 0$ ${}^{g}u_6 - {}^{g}u_{12} = 0$	${}^{g}F_4 + {}^{g}F_7 + {}^{g}F_{10} =$ 0 ${}^{g}F_5 + {}^{g}F_8 + {}^{g}F_{11} =$ 0 ${}^{g}F_6 + {}^{g}F_9 + {}^{g}F_{12} - M = 0$
C	${}^{g}u_{16} = 0$ ${}^{g}u_{19} = 0$ ${}^{g}u_{17} =$ 0 ${}^{g}u_{20} = 0$ ${}^{g}u_{18} - {}^{g}u_{21} = 0$	${}^{g}F_{18} + {}^{g}F_{21} = 0$
D	${}^{g}u_{22} - {}^{g}u_{25} = 0$ ${}^{g}u_{23} - {}^{g}u_{26} =$ 0 ${}^{g}u_{24} - {}^{g}u_{27} = 0$	${}^{g}F_{22} + {}^{g}F_{25} = 0$ ${}^{g}F_{23} + {}^{g}F_{26} + F_y =$ 0 ${}^{g}F_{24} + {}^{g}F_{27} = 0$
E	${}^{g}u_{13} - {}^{g}u_{28} = 0$ ${}^{g}u_{13} - {}^{g}u_{31} =$ 0 ${}^{g}u_{14} - {}^{g}u_{29} =$ 0 ${}^{g}u_{14} - {}^{g}u_{32} =$ 0 ${}^{g}u_{15} - {}^{g}u_{30} =$ 0 ${}^{g}u_{15} - {}^{g}u_{33} = 0$	${}^{g}F_{13} + {}^{g}F_{28} + {}^{g}F_{31} - F_x =$ 0 ${}^{g}F_{14} + {}^{g}F_{29} + {}^{g}F_{32} =$ 0 ${}^{g}F_{15} + {}^{g}F_{30} + {}^{g}F_{33} = 0$

Undoubtedly, the use of the analytical solutions of the kinematics greatly reduces the time required for the formation of the objective function vector if compared with the numerical approach, which requires to carry out numerical integrations at every iteration.

Whatever is the way to face kinematics, the nodal forces at the "J" beam nodes are analytically linked to the forces at the nodes "I" simply using equilibrium through Eq. (13).

As shown in the previous examples, the vector of objective functions collects equations that refer to different physical quantities, displacements and forces. It is useful to partition Eq. (52) separating the rows $\{\Phi_u\}$ concerning displacement constraints from those regarding forces $\{\Phi_F\}$:

$$\{\Phi(\{\boldsymbol{F}_I\},\{\boldsymbol{u}_I\})\} = \begin{Bmatrix} \{\Phi_u(\{\boldsymbol{F}_I\},\{\boldsymbol{u}_I\})\} \\ \{\Phi_F(\{\boldsymbol{F}_I\},\{\boldsymbol{u}_I\})\} \end{Bmatrix}_{n_{DOFs}\times 1} = \{0\} \tag{56}$$

Due to structural stiffness, the displacement constraints $\{\Phi_u\}$ need to be respected with a more restrictive tolerance criterion than forces require. Therefore, a parameter $\lambda \gg 1$ is introduced to weigh the residuals due to kinematic constraints more than those due to force unbalances when evaluating the objective function norm at the k^{th} iteration:

$$\|\Phi^k\| = \sqrt{\lambda\{\Phi_u{}^k\}^T\{\Phi_u{}^k\} + \{\Phi_F{}^k\}^T\{\Phi_F{}^k\}} \tag{57}$$

Whatever algorithm is used to solve Eq. (56), the procedure converges when the norm of the objective function vector is less than a threshold value $\|\Phi^k\| \leq Tol$. Additional information regarding the algorithm used by the authors to address the problem are discussed in §5.

It is worth to highlight that the rows of $\{\Phi_u\}$ associated to external (to the ground) kinematic constraints are respected *a priori*. Furthermore, it is also possible to find the solution with imposed displacements, which are treated in $\{\Phi_u\}$ as imposed kinematic constraints and therefore also respected *a priori*.

The formulation of the optimization problem discussed in this paper presents some peculiar aspects. The objective functions of Eq. (56) form a non-linear system, hence, the optimization problem turns out into the search for zeros of a nonlinear system. This is an important feature, as it allows you to quantify how the obtained solution is correct, simply checking its proximity to zero norm; the presented formulation differs from classical optimization problems where the objective is to achieve

the minimum of a functional, but it is not possible to verify the quality of the solution inasmuch it is not possible to verify whether the solution obtained is an absolute or local minimum. Although the main purpose is to achieve uniform-strength, the developed procedure assumes it as always verified, since the uniform-strength condition is analytically embedded into Eq. (52), and the objective is the satisfaction of the kinematic congruence and forces balance. Thanks to this approach, the search for the optimum results as an unconstrained optimization problem in which all the beams have a uniform-strength shape, but the resultant design solutions are the only ones that fulfill both equilibrium and kinematic congruence. Undoubtedly, the feature of having an unconstrained optimization is of particular importance because it allows the computational efforts to be greatly reduced.

It is worth to point out that, due to the high nonlinearity of the system in Eq. (56), the solution may not be unique; more specifically, the solution is affected by the choice of the starting (trial) solution that is provided to the algorithm. As described in the next section (§5) a good choice is to start the algorithm with a trial solution, in terms of forces and moments, obtained from a structure with beams all having the same cross-section dimensions. This allows to achieve a homogeneous optimal solution in terms of shape of the beams, i.e. avoiding configurations in which the beams show very different sizes at the connection points.

5. Examples, robustness and required computational effort vs DOFs

This section shows some examples of optimized uniform-strength structures, with the aim to show the performance, reliability and robustness of the proposed procedure. As previously mentioned, the results consider only shape optimizations, non-modifying the layout and topology of the baseline structure (before optimization).

As described in §4, the optimized shapes carry out from the solution of the non-linear system of Eq. (56), which represents the objective functions imposing the kinematic and force boundary balancing. The zeros of Eq. (56) can be obtained using various methods; in the presented examples the trust-region method [17,71] is adopted, enhanced by parallel computing. The optimal solutions are achieved setting a relative tolerance on force balance equal to 10^{-4} and a weight parameter $\lambda = 10^2$ (resulting a relative tolerance of 10^{-6} on generalized displacements).

To start the procedure a trial solution is required; as usually in non-linear programming, this is a delicate issue. In order not to make this choice random or case-dependent, we carry out a linear elastic Finite Element Analysis (FEA) on the baseline structure with all cross-sections set to constant unique shape; the obtained displacements and forces provide a first attempt for the optimization progress. This starting criterion has always proven to be effective and led to solutions with much fewer iterations if comparing to any other generation of the trial solution. As expected, being Eq. (56) a non-linear system, the solution could not be unique, i.e. different trial solutions can generate dissimilar optimal results.

All examples discussed involve statically-indeterminate structures. The material is elastic, homogeneous and isotropic with $E = 200GPa$. The geometrical dimensions and applied forces are given, for each case, on the relative figures.

The effective achievement of uniform strength is evaluated, in terms of stress distribution, performing a linear FEA on the optimized structure with several beam elements, so that the shape variability is assumed. Of course, this verification is worthy because the FEA involves the fulfillment of the kinematic congruence.

Fig. 9 shows a straight structure having hollow circular sections with void ratio $\alpha = 0.5$. The structure is subjected to two concentrated forces, transverse and axial, together with a constant distributed load. The presence of the distributed and axial forces infers the formation of the objective function vector through the numerical integration of Eqs.

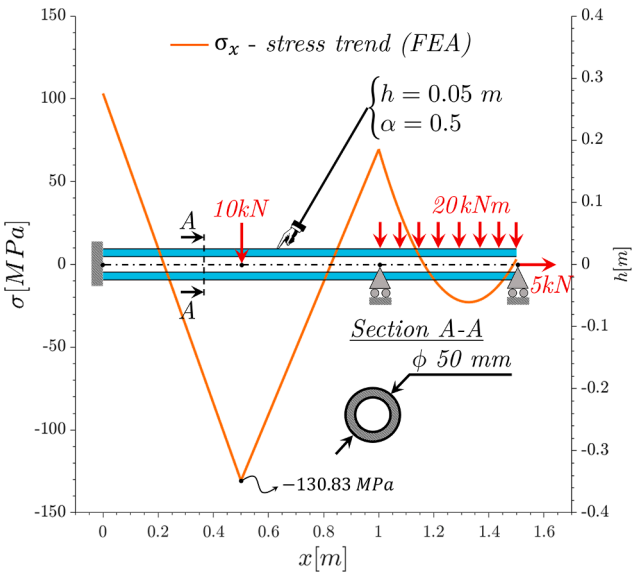

Fig. 9. Straight structure formed by circular beams with constant cross-sections.

(48–50). The maximum stress on the baseline structure of Fig. 9 presents a magnitude of $\approx 130MPa$. This maximum value is taken as the uniform strength stress σ_{max} to perform the optimization of the structure, shown in Fig. 10; in this figure are reporter the bending moments and axial forces trends along each beams, which can be used into the Eqs. (22,23) to build-up the analytical shapes of the optimized beams. To check the resulting shape at the end of the optimization process a FEA was performed; its maximal stress distribution is visible in Fig. 10 and it confirms the accuracy of.

the optimized solution. The regions immediately close to sudden cross-section restrictions present less accurate results in terms of uniform strength, due to their dependency on FE mesh sizing and the imposed minimal thickness of $2.25mm$ to perform the FEA. This last minimal thickness is given to guarantee the strength to shear and axial forces when bending moments vanish.

Fig. 11 shows a frame structure made of beams with square cross sections, subjected only to concentrated forces and moments. For this case the optimization is carried out using the analytical solutions of Eqs. (45–47), valid for homothetic sections. The optimized result is shown at the right end of Fig. 11, obtained setting the uniform strength stress at $150MPa$, higher than the maximum stress of $114MPa$ experienced by the baseline structure. It is worth to highlight that all results, i.e. the shape and weight of the structures, are dependent on the chosen value of the uniform strength stress. To delve into this, Fig. 12 shows the relationship between the structure weights and the fixed uniform strength stresses, which defines a Pareto frontier, so that the minimum possible weight at that stress value. In other words, if the weight limitation is a purpose to reach, this can be achieved performing a number of optimization attempts, determining the association between weight and uniform strength stress. Furthermore, Fig. 12 show a reference for a direct comparison in terms of total weight if the maximum value of the stress experienced by the baseline structure (114 MPa) is enforced in the optimized structure. In this particular case the total weight is reduced quite two times (196 %), but much better reduction can be achieved if the allowable stress is furtherly increased.

A more geometrically heterogeneous example is the structure of Fig. 13, starting from a solid structure to obtain a frame version to optimize. The solid structure in Fig. 13a is the well-known shape of a uniform strength cantilever beam with constant width, subjected to a transversal force at the end; this shape offers *iso*-stress only at top and bottom edges, presenting less-and-less loaded material approaching the

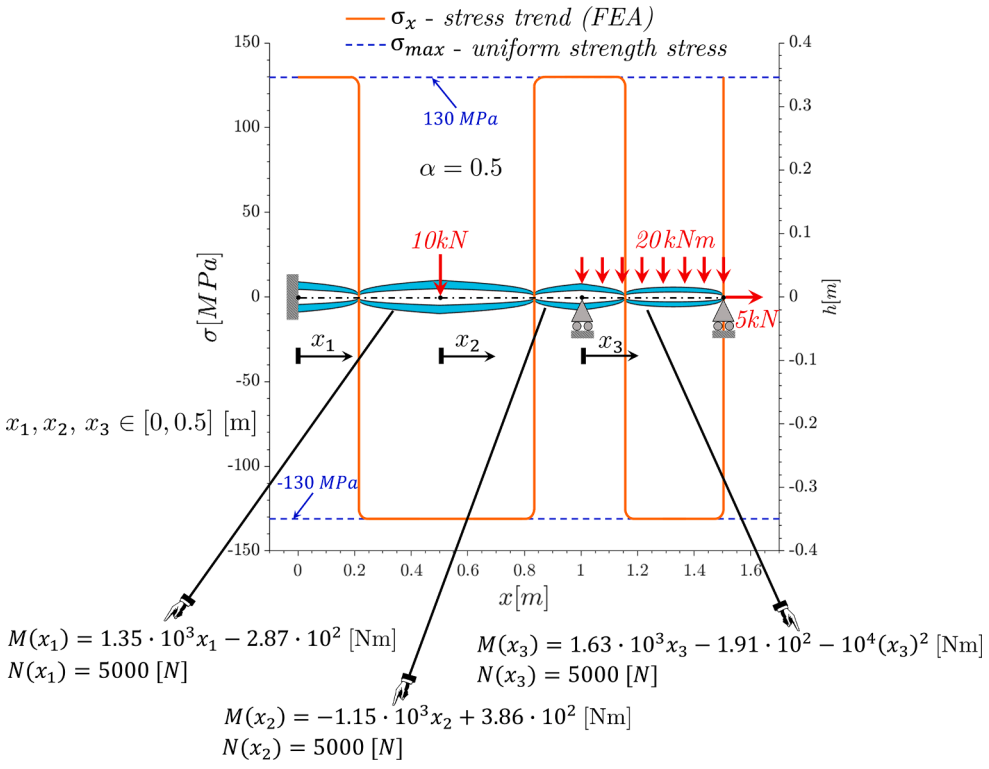

Fig. 10. Optimization of the straight structure in Fig. 9 taking into account axial and distributed forces.

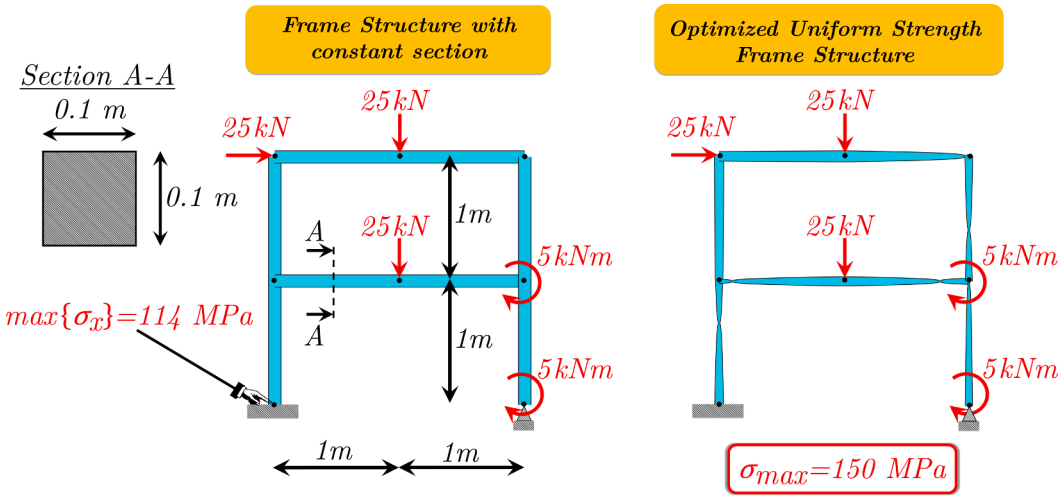

Fig. 11. Constant section frame structure and its optimized uniform-strength shape.

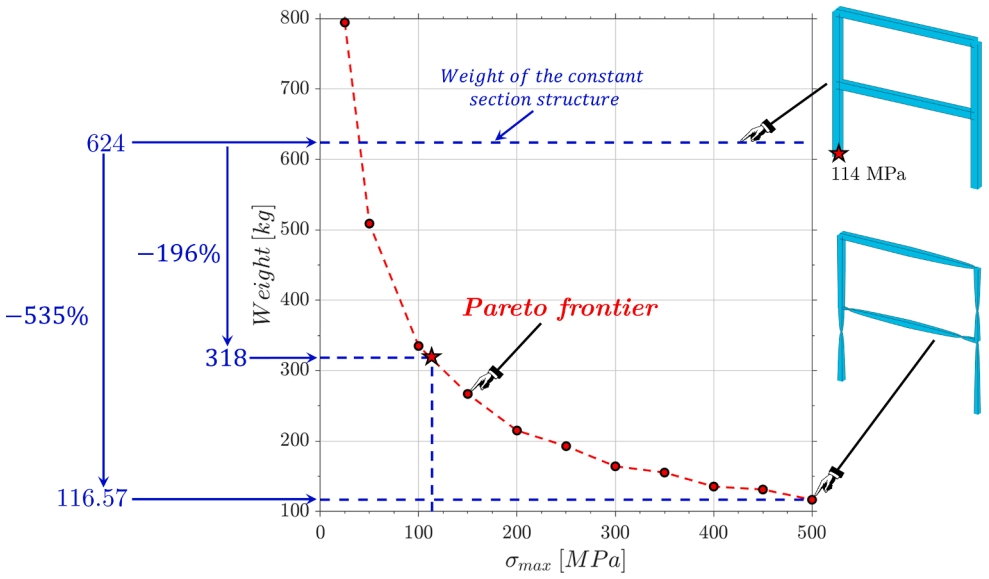

Fig. 12. Volume of the optimized structure as function of the uniform-strength stress.

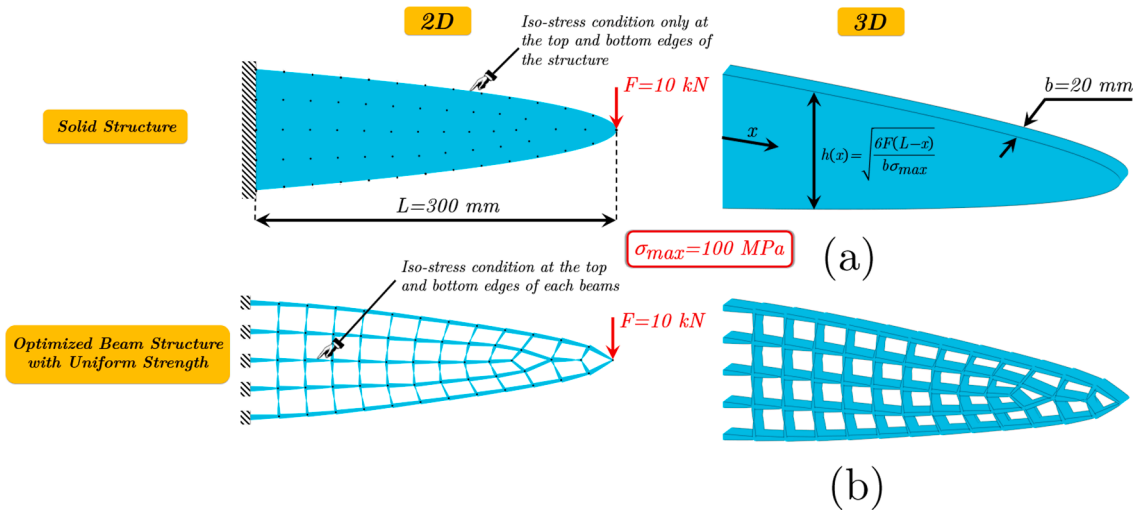

Fig. 13. Optimization of the cantilever solid-structure (a), to obtain the uniform-strength cantilever beam-structure (b).

cross-section centers. To achieve the optimized geometry using the analytical solution of Eqs. (34–36), we first discretize the solid structure with a mesh of 62 nodes (Fig. 13a) and 103 beams and compute the trial solution with rectangular beams having constant cross-sections of $3 \times 20mm^2$.

The optimized structure in Fig. 13b, in which the weight is the 17.4 % of the initial solid cantilever, turns out to be lighter and more efficient since all the beams offer the *iso*-stress condition of 100 MPa at top and bottom edges.

Other design solutions can be obtained changing the initial topology, i.e. with a different meshing of the solid structure.

The presented procedure results especially suitable to optimize machine components; in this regard, in Fig. 14 is addressed the case of a torsional joint. The solid torsional joint, whose geometric measurements are shown in Fig. 14a, is internally fixed and subject to a torque of 1.6 kNm on the outer crown. To obtain a lighter as well uniform-strength joint, the solid structure is discretized with a mesh of 144 nodes (Fig. 14a) to form an ordered lattice structure of 324 beams. The optimized result in Fig. 14b, having a weight of 23.8 % of the initial solid joint and.

an *iso*-stress of 130 MPa, is obtained starting from a trial configuration with rectangular beams having constant cross-sections of $2 \times 50mm^2$. It is interesting to point out that despite the solution being computed considering the entire structure, the solution appears almost perfectly symmetrical; however, it is a result, not an imposition.

Two structures in Fig.s 15 and 16 are proposed to test the procedure in terms of robustness and computational effort when DOF numbers increase. The interest embraces both a linear development as well as a planar one. To accomplish this, a supported (Fig. 15) and a frame (Fig. 16) structure are given, with circular and square sections, respectively. Both structures, together with constraints and loads, may be repeated sequentially several times.

Fig. 17 shows the trend of the computational time required to reach the solutions as a function of the DOF numbers – up to 6000 so that 36,000 unknowns – using the analytical solutions of §3. The time consumed is reported in ordinate, making it dimensionless referring to the case with 120 DOFs for the supported structure, and 144 DOFs for the frame one. Downstream of these tests, that always reached convergence, it is possible to confirm that the procedure is robust, including the criterion to choose the trial solution. The required computational effort

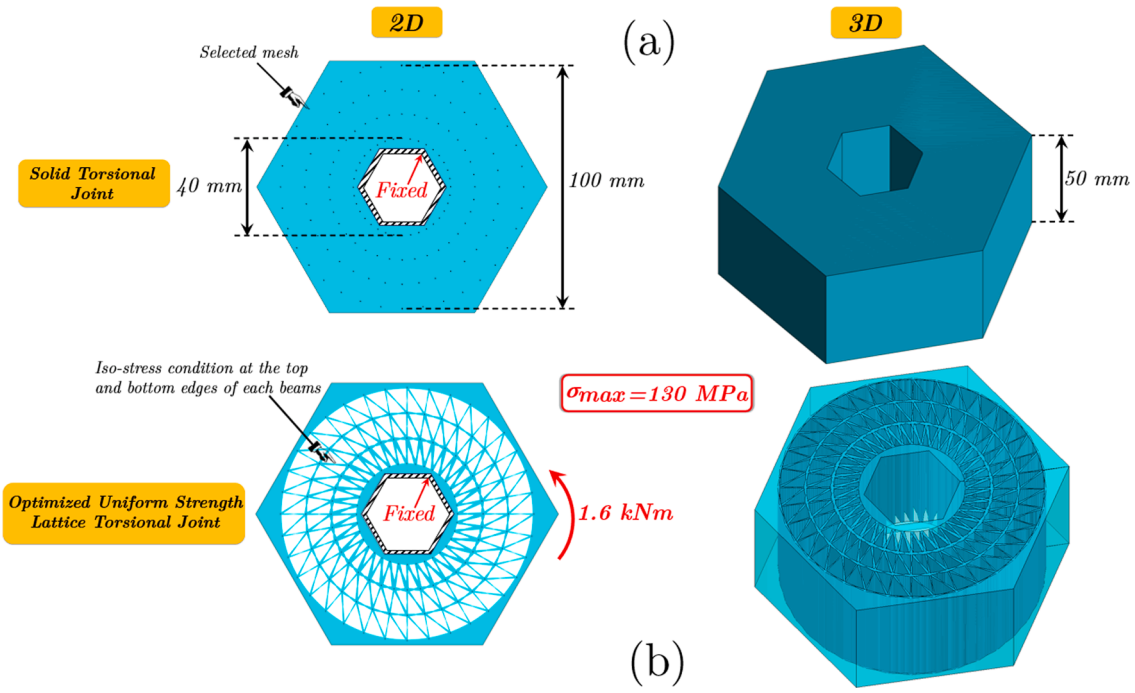

Fig. 14. Optimization the solid torsional joint (a), to obtain the uniform-strength lattice torsional joint (b).

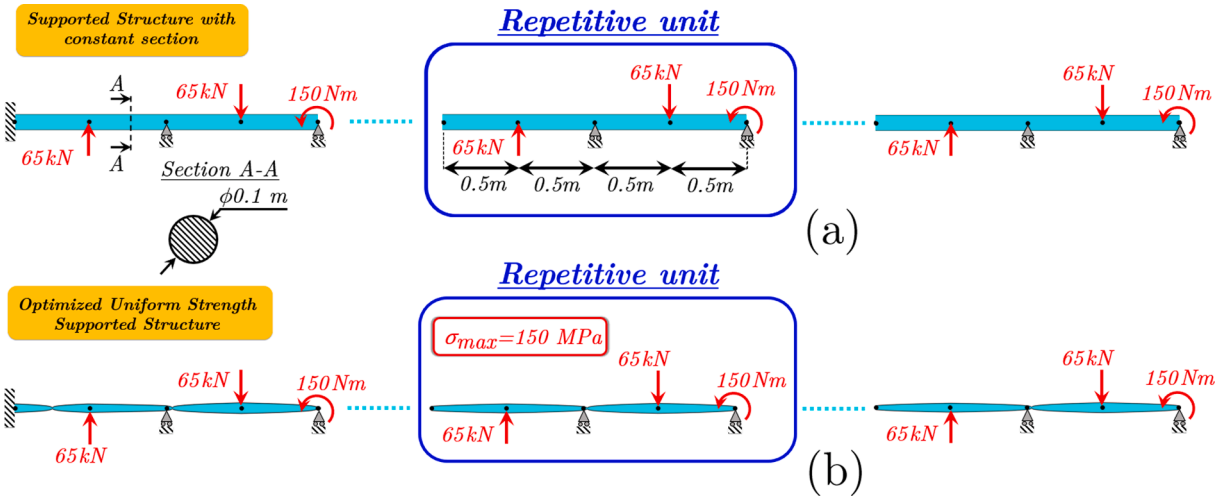

Fig. 15. Optimization of a supported structure with repetitive units.

trend of Fig. 17 shows that the optimization, involving here the search of zeros of a non-linear system, is affected by the size of the model in a reasonable way, in accordance with the increase of classical optimization problems presented in literature.

6. Conclusions

This paper presents a shape optimization procedure to obtain the uniform strength of planar frames or lattice structures (statically-indeterminate) made of beam elements. Uniform strength condition is enforced for the entire structure since this condition entails the best material utilization, which results in weight minimization. The proposed optimization procedure is particularly suitable in applications where weight reduction is paramount, as for automotive and aerospace industries, more generally for machine components.

The beams forming the frames follow the one-dimensional Timoshenko model, and the beams shape, fixed the form of the cross-section, are the variables of the optimization process. Two types of sections are analysed, rectangular with fixed width, and homothetic ones (circular, square, etc.); for all these sections the beam shape is analytically defined by means of geometric coefficients. Further beam-shapes with different cross-section types can be obtained following the same analytical workflow.

The forces-displacements behaviour of the uniform strength beam is analytically deduced for concentrated end-loads; for distributed loads the determination of the forces-displacements behaviour needs a numerical approach that in this paper is generalized to also address any section and beam shape. Since the uniform-strength beam shape is a function of the nodal forces, the force–displacement relationships appear as highly non-linear.

The analytical formulation of the problem allows to directly insert the uniform strength condition into the kinematics equations. This approach allows the optimization problem subject to uniform strength constraint to be transformed into an unconstrained problem in which all

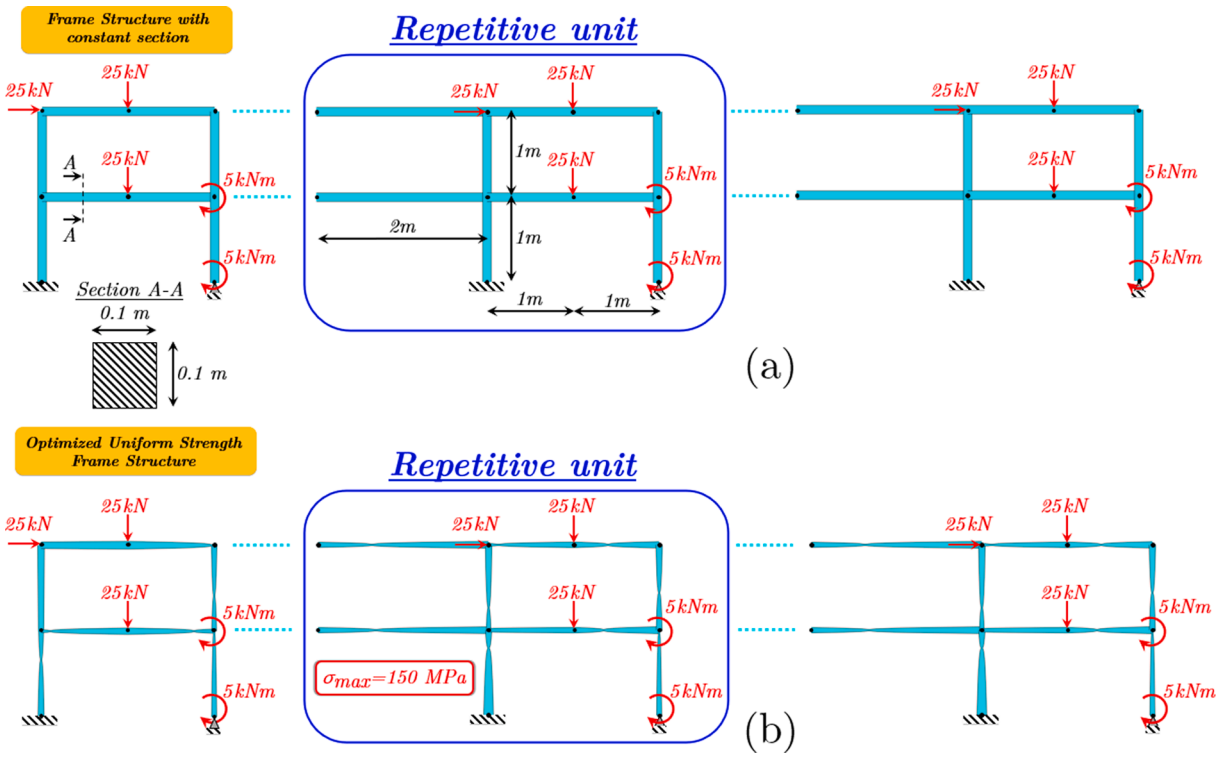

Fig. 16. Optimization of a frame structure with repetitive units.

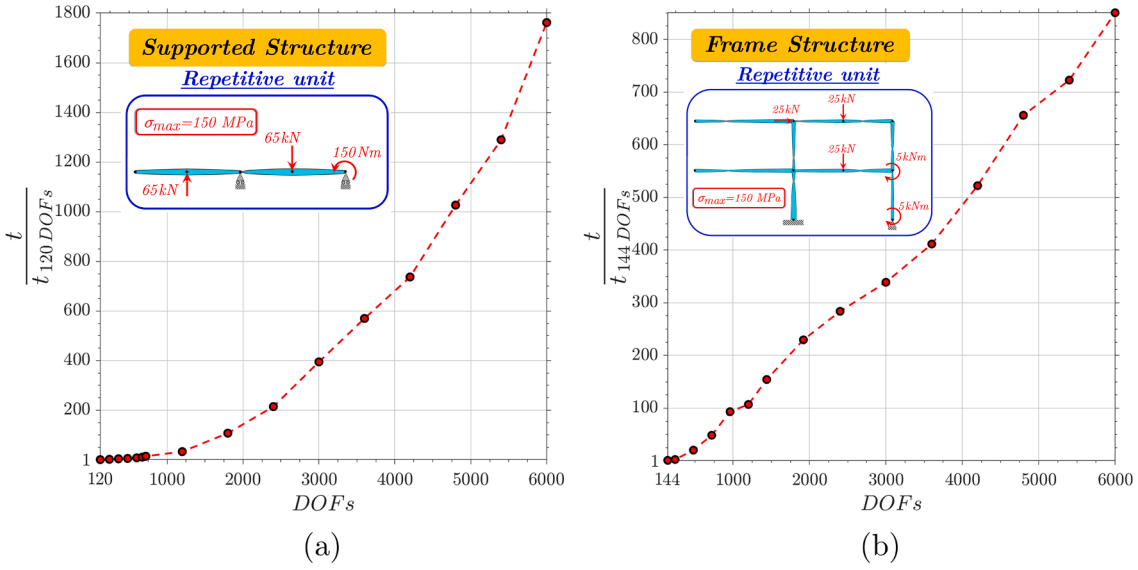

Fig. 17. Relative time to perform the optimization of the repetitive: (a) supported structures and (b) frame structure.

beam shapes are *iso*-resistant, but the optimized solutions are the only ones that respect both equilibrium and kinematic congruence.

Therefore, the addressed objective functions become the conditions of kinematic-congruence and force balance to be fulfilled at every node of the structure and the optimization problem turns into the search for the zeros of a non-linear system. Furthermore, this formulation of the optimization problem allows to quantify how the obtained solution is exact simply checking its proximity to zero norm.

Clearly, being the problem highly nonlinear, the solution is not unique and it depends on the starting (trial) solution.

The most important feature of the procedure is that each row of the objective-functions vector is analytically assembled, allowing to avoid the recurring to any external computation, e.g. FEA, for the updating of the optimization workspace at each iteration, as often necessary in many structural optimization workflows. This feature significantly reduces the computational time required by the optimization process.

The presented optimization procedure is made evident through some examples. Its robustness and applicability on structures made with thousands of elements is proven, with examples involving an increasing number of DOFs. The reliability of the optimization process is verified performing FEA analysis on the optimized structures, checking that the stress distribution satisfies the uniform strength condition.

CRediT authorship contribution statement

Christian Iandiorio: Writing – review & editing, Writing – original draft, Visualization, Validation, Supervision, Software, Methodology, Investigation, Data curation, Conceptualization. **Daniele Milani:** Validation, Software, Investigation, Conceptualization. **Pietro Salvini:** Writing – review & editing, Writing – original draft, Supervision, Methodology, Investigation, Conceptualization.

Declaration of competing interest

The authors declare that they have no known competing financial interests or personal relationships that could have appeared to influence the work reported in this paper.

Data availability

Data will be made available on request.

Appendix

A. Uniform-strength solution for homothetic sections with a negative cubic discriminant

The physical acceptable solution of the cubic Eq. (21) with a negative discriminant (Eq. (22)) is the unique positive solution of the following equation:

$$h(x) = 2\sqrt{\frac{|N(x)|}{c_A \sigma_{max}}}\cos\left(\frac{\vartheta + 2\pi(k-1)}{3}\right) \tag{A1}$$

with $k \in (1,2,3)$ and $\vartheta = atan2\left(-\frac{|M(x)|}{4c_I\sigma_{max}}\right)$.

References

[1] Arora JS, Wang Q. Review of formulations for structural and mechanical system optimization. Struct Multidisc Optim 2005;30:251–72. https://doi.org/10.1007/s00158-004-0509-6.

[2] Wu J, Sigmund O, Groen JP. Topology optimization of multi-scale structures: a review. Struct Multidisc Optim 2021;63:1455–80. https://doi.org/10.1007/s00158-021-02881-8.

[3] Kaveh A, Talatahari S. Charged system search for optimal design of frame structures. Appl Soft Comput 2012;12:382–93. https://doi.org/10.1016/j.asoc.2011.08.034.

[4] Lamberti L, Pappalettere C. Design optimization of large-scale structures with sequential linear programming. J Mech Eng Sc 2002;216(8):799–811. https://doi.org/10.1243/09544060260171438.

[5] Jiang C, Tang C, Seidel HP, Wonka P. Design and volume optimization of space structures. 159 1–14 ACM Trans Graph 2017;36(4). https://doi.org/10.1145/3072959.3073619.

[6] Chai S, Chen B, Ji M, Yang Z, Lau M, Fu XM, et al. Stress-oriented structural optimization for frame structures. Graph Model 2018;97:80–8. https://doi.org/10.1016/j.gmod.2018.04.002.

[7] Degertekin SO, Lamberti L, Ugur IB. Sizing, layout and topology design optimization of truss structures using the Jaya algorithm. Appl Soft Comput 2018;70:903–28. https://doi.org/10.1016/j.asoc.2017.10.001.

[8] Ma Y, Song X, Jia Q, Zhao Y, Lu S. Isogeometric interval size optimization of beam structures. Comp Meth Appl Mech Eng 2022;395:115003. https://doi.org/10.1016/j.cma.2022.115003.

[9] Zhang X, Xie YM, Zhou S. A nodal-based evolutionary optimization algorithm for frame structures. Comp Aid Civ Infras Eng 2022;38(3):288–306. https://doi.org/10.1111/mice.12834.

[10] Kaveh A, Mirzaei B, Jafarvand A. An improved magnetic charged system search for optimization of truss structures with continuous and discrete variables. Appl Soft Comput 2015;28:400–10. https://doi.org/10.1016/j.asoc.2014.11.056.

[11] Asadpoure A, Valdevit L. Topology optimization of lightweight periodic lattices under simultaneous compressive and shear stiffness constraints. Int J Sol Struct 2015;60–61:1–16. https://doi.org/10.1016/j.ijsolstr.2015.01.016.

[12] Chao L, Yaoyao S. Comprehensive structural analysis and optimization of the electrostatic forming membrane reflector deployable antenna. Aerosp Sci Technol 2016;53:267–79. https://doi.org/10.1016/j.ast.2016.03.026.

[13] Rashid R, Masood SH, Ruan D, Palanisamy S, Huang X, Rahman Rashid RA. Topology Optimisation of Additively Manufactured Lattice beams for three-point bending test. 29th Ann Int Sol Freef Fabr Symp 2018. https://doi.org/10.26153/tsw/17066.

[14] Pan C, Han Y, Lu J. Design and Optimization of Lattice Structures: A Review. Appl Sci 2020;10:6374. https://doi.org/10.3390/app10186374.

[15] Wang Y, Li S, Yu Y, Xin Y, Zhang X, Zhang Q, et al. Lattice structure design optimization coupling anisotropy and constraints of additive manufacturing. Mater Des 2020;196:109089. https://doi.org/10.1016/j.matdes.2020.109089.

[16] Toragay O, Silva DF, Vinel A, Shamsae N. Exact global optimization of frame structures for additive manufacturing. Struct Mult Opt 2022;65(97). https://doi.org/10.1007/s00158-022-03178-0.

[17] Nocedal J, Wright SJ. Numerical Optimization. Springer Series in Operations Research and Financial Engineering, Springer 2006. ISBN: 978-0-387-30303-1.

[18] Lee KY, El-Sharkawi MA. Modern Heuristic Optimization Techniques: Theory and Applications to Power Systems. Wiley-IEEE Press 2008. ISBN: 978-0471457114.

[19] Yang XS. Nature-Inspired Optimization Algorithms. Elsevier; 2014.

[20] Kaveh A. Advances in Metaheuristic Algorithms for Optimal Design of Structures. Springer Cham, 2014.

[21] Lamberti L, Pappalettere C. Improved sequential linear programming formulation for structural weight minimization. Comput Methods Appl Mech Engrg 2004;193:3493–521. https://doi.org/10.1016/j.cma.2003.12.040.

[22] Mosharmovahhed M, Moharram H. Design optimization of moment frame structures by the method of inscribed hyperspheres. Struct Multidisc Optim 2021;64:335–48. https://doi.org/10.1007/s00158-021-02869-4.

[23] Chernyaev YA. Gradient Projection Method for a Class of Optimization Problems with a Constraint in the Form of a Subset of Points of a Smooth Surface. Comp Math Math Phys 2021;61:368–75. https://doi.org/10.1134/S0965542521020068.

[24] Katoch S, Chauhan SS, Kumar V. A review on genetic algorithm: past, present, and future. Mult Tools Appl 2021;80:8091–126. https://doi.org/10.1007/s11042-020-10139-6.

[25] Tsiptsis IN, Liimatainen L, Kotnik T, Niiranen J. Structural optimization employing isogeometric tools in Particle Swarm Optimizer. J Build Eng 2019;24:100761. https://doi.org/10.1016/j.jobe.2019.100761.

[26] Sych P, Słoński M. Structural Design Optimization of Steel Beams and Frames with Web-Tapered Members Using the PSO-FEM Algorithm. Comp Ass Meth Eng Sc 2021;28(1):39–55. https://doi.org/10.24423/cames.284.

[27] Aydoğdu İ, Saka MP. Ant colony optimization of irregular steel frames including elemental warping effect. Adv Eng Soft 2012;44(1):150–69. https://doi.org/10.1016/j.advengsoft.2011.05.029.

[28] Greco A, Pluchino A, Cannizzaro F. An improved ant colony optimization algorithm and its applications to limit analysis of frame structures. Eng Opt 2018;51(1). https://doi.org/10.1080/0305215X.2018.1560437.

[29] Porziani S, De Crescenzo F, Lombardi E, Iandiorio C, Salvini P, Automatic BME, et al. Lecture Notes in Computer Science 2021; 12746. Springer, Cham 2021. https://doi.org/10.1007/978-3-030-77977-1_38.

[30] Xie YM, Steven GP. A simple evolutionary procedure for structural optimization. Comp Struct 1993;49(5):885–96. https://doi.org/10.1016/0045-7949(93)90035-C.

[31] Steven G, Querin O, Xie M. Evolutionary structural optimisation (ESO) for combined topology and size optimisation of discrete structures. Comput Methods Appl Mech Engrg 2000;188:743–54. https://doi.org/10.1016/S0045-7825(99)00359-X.

[32] Stromberg LL, Beghini A, Baker WF, Paulino GH. Topology optimization for braced frames: Combining continuum and beam/column elements. Eng Struct 2012;37:106–24. https://doi.org/10.1016/j.engstruct.2011.12.034.

[33] Lian H, Christiansen AN, Tortorelli DA, Sigmund O, Aage N. Combined Shape and Topology Optimization for Minimization of Maximal von Mises Stress. Struct Mult Opt 2017;55:1541–57. https://doi.org/10.1007/s00158-017-1656-x.

[34] Kozikowska A. Geometry and Topology Optimization of Statically Determinate Beams under Fixed and Most Unfavorably Distributed Load. Lat Am J Solids Struct 2016;13(4). https://doi.org/10.1590/1679-78252306.

[35] Ohsaki M, Hayashi K. Force density method for simultaneous optimization of geometry and topology of trusses. Struct Multidisc Optim 2017;56:1157–68. https://doi.org/10.1007/s00158-017-1710-8.

[36] An H, Huang H. Topology and Sizing Optimization for Frame Structures with a Two-Level Approximation Method. AIAA J 2017;55(3). https://doi.org/10.2514/1.J055020.
[37] Larsen SD, Sigmund O, Groen JP. Optimal truss and frame design from projected homogenization-based topology optimization. Struct Multid Optim 2018;57:1461–74. https://doi.org/10.1007/s00158-018-1948-9.
[38] Shimoda M, Tani S. Simultaneous shape and topology optimization method for frame structures with multi-materials. Struct Multid Optim 2021;64:699–720. https://doi.org/10.1007/s00158-021-02871-w.
[39] Laghi V, Palermo M, Bruggi M, Gasparini G, Trombetti T. Blended structural optimization for wire–and–arc additively manufactured beams. Progress in Additive Manufacturing 2022;8:381–92. https://doi.org/10.1007/s40964-022-00335-1.
[40] Changizi N, Amir M, Warn G, Papakonstantinou KG. Topology optimization of structural frames based on a nonlinear Timoshenko beam finite element considering full interaction. Int J Num Meth Eng 2022;123(19):4562–85. https://doi.org/10.1002/nme.7046.
[41] Taylor JE. On the Prediction of Structural Layout for Maximum Stiffness. J Optim Theory Appl 1975;15(1). https://doi.org/10.1007/BF00933027.
[42] Wang D, Zhang WH, Jiang JS. Truss shape optimization with multiple displacement constraints. Comput Methods Appl Mech Engrg 2002;191:3597–612. https://doi.org/10.1016/S0045-7825(02)00297-9.
[43] Wang D. Optimal shape design of a frame structure for minimization of maximum bending moment. Eng Struct 2007;29:1824–32. https://doi.org/10.1016/j.engstruct.2006.10.004.
[44] Fraternali F, Marino A, El Sayed T, Della CA. On the Structural Shape Optimization through Variational Methods and Evolutionary Algorithms. Mech Adv Mat Struct 2011;18:225–43. https://doi.org/10.1080/15376494.2010.483319.
[45] Shimoda M, Liu Y, Morimoto T. Non-parametric free-form optimization method for frame structures. Struct Multidisc Optim 2014;50:129–46. https://doi.org/10.1007/s00158-013-1037-z.
[46] Pezeshk S. Design of Framed Structures: an Integrated Non-Linear Analysis and Optimal Minimum Weight Design. Int J Num Meth Eng 1998;41:459–71. https://doi.org/10.1002/(SICI)1097-0207.
[47] Nagy AP, Abdalla MM, Gürdal Z. Isogeometric sizing and shape optimisation of beam structures. Comput Methods Appl Mech Engrg 2010;199:1216–30. https://doi.org/10.1016/j.cma.2009.12.010.
[48] Tyburec M, Zeman J, Kružík M, Henrion D. On Optimum Design of Frame Structures. Acta Polytechnica CTU Proceedings 2020;26:117–25. https://doi.org/10.14311/APP.2020.26.0117.
[49] Huang NC. Optimal design of elastic structures for maximum stiffness. Int J Sol Struct 1968;4:689–700. https://doi.org/10.1016/0020-7683(68)90070-X.
[50] Masur EF. Optimum stiffness and strength of elastic structures. J Eng Mech Div ASCE EM 1970;5:621–49. https://doi.org/10.1061/JMCEA3.000127.
[51] Banichuk NV, Barsuk AA. Design of an optimum column with elastic clamping. Struct Multidisc Optim 1995;9:254–7. https://doi.org/10.1007/BF01743979.
[52] Seyranian AP, Privalova OG. The Lagrange problem on an optimal column: old and new results. Struct Multidisc Optim 2003;25:393–410. https://doi.org/10.1007/s00158-003-0333-4.
[53] Pedersen P, Pedersen NL. Analytical optimal designs for long and short statically determinate beam structures. Struct Multidisc Optim 2009;39:343–57. https://doi.org/10.1007/s00158-008-0339-z.
[54] Abdalla HMA, Casagrande D. Optimal area variation for maximum stiffness isostatic beams under parametric linear distributed loads. Mech Res Comm 2021;111:103659. https://doi.org/10.1016/j.mechrescom.2021.103659.
[55] Lewis WJ. Constant stress arches and their design space. Proc R Soc A 2021;478:20210428. https://doi.org/10.1098/rspa.2021.0428.
[56] Rasiya G, Shukla A, Saran K. Additive Manufacturing-A Review. Mater Today: Proc 2021;47(19):6896–901. https://doi.org/10.1016/j.matpr.2021.05.181.
[57] Srivastava M, Rathee S, Patel V, Kumar A, Koppad PG. A review of various materials for additive manufacturing: Recent trends and processing issues. J Mater Res Technol 2022;21:2612–41. https://doi.org/10.1016/j.jmrt.2022.10.015.
[58] Armstrong M, Mehrabi H, Naveed N. An overview of modern metal additive manufacturing technology. J Manuf Process 2022;84:1001–29. https://doi.org/10.1016/j.jmapro.2022.10.060.
[59] Abdalla HMA, Casagrande D. Direct Transcription Approach to Dynamic Optimization Problems in Engineering. J Appl Comput Mech 2022;8(2):605–16. https://doi.org/10.22055/JACM.2021.38081.3150.
[60] Timoshenko SP. Strength of Materials (parts I & II). D. Van Nostrand Company, 1940.
[61] Brandt AM. Criteria and Methods of Structural Optimization. Dordrecht: Springer; 1984.
[62] Mattheck C. Design in Nature: Learning from Trees. Berlin: Springer; 1998.
[63] Azegami H. A Proposal of a Shape-Optimization Method Using a Constitutive Equation of Growth. J Soc Mech Eng Part C 1988;54(508). https://doi.org/10.1299/kikaia.54.2167.
[64] Azegami H, Ogihara T, Takami A. Analysis of Uniform-Strength Shape by the Growth-Strain Method. J Soc Mech Eng Part C 1991;34(3). https://doi.org/10.1299/kikaic.56.589.
[65] Iandiorio C, Salvini P. An Engineering Theory of thick Curved Beams loaded in-plane and out-of-plane: 3D Stress Analysis. Eur J Mech - A/Solids 2022;92:104484. https://doi.org/10.1016/j.euromechsol.2021.104484.
[66] Love AEH. A Treatise on the Mathematical Theory of Elasticity. Cambridge University Press; 1892.
[67] Iandiorio C, Salvini P. Elastic-plastic analysis with pre-integrated beam finite element based on state diagrams: Elastic-perfectly plastic flow. Eur J Mech - A/Solids 2023;97:104837. https://doi.org/10.1016/j.euromechsol.2022.104837.
[68] Iandiorio C, Salvini P. Elasto-Kinematics and Instantaneous Invariants of Compliant Mechanisms Based on Flexure Hinges. Micromachines 2023;14:783. https://doi.org/10.3390/mi14040783.
[69] Iandiorio C, Salvini P. Shape optimization of 2D beam-structures to obtain the uniform-strength. IOP Conf Ser: Mater Sci Eng 2023;1275:012030. https://doi.org/10.1088/1757-899X/1275/1/012030.
[70] Abramowitz M, Stegun IA. Handbook of Mathematical Functions with Formulas, Graphs, and Mathematical Tables (9th printing). Dover 1972, New York.
[71] Conn AR, Gould NIM, Toint PL. Trust Region Methods. Society for Industrial and Applied Mathematics 2000. ISBN: 978-0-898714-60-9.